Table 5 Tacrolimus dose and exposure parameters over time in adult LDLT patients according to donor's and recipient's *CYP3A5* genotypes

	Donor		Recipient	
Time posttransplantation	*3/*3 (n=36)	*1/*1 and *1/*3 (n=24)	*3/*3 (n=40)	*1/*1 and *1/*3 (n=20)
Day 7				
Daily dose (mg/kg)	0.037±0.025	0.057±0.030[a]	0.041±0.030	0.054±0.023[a]
C_0 (ng/ml)	10.8±4.2	11.1±3.8	11.1±3.9	10.6±4.2
C/D ratio [(ng/ml)/(mg/kg)]	454±320	217±118[a]	414±324	256±137[a]
Day 14				
Daily dose (mg/kg)	0.057±0.032	0.074±0.051	0.054±0.034	0.083±0.049[a]
C_0 (ng/ml)	9.5±3.1	9.5±3.5	9.7±3.3	9.1±3.0
C/D ratio [(ng/ml)/(mg/kg)]	228±148	222±188	251±167	178±148[a]
Month 1				
Daily dose (mg/kg)	0.051±0.033	0.086±0.046[a]	0.061±0.042	0.082±0.043
C_0 (ng/ml)	8.5±2.7	8.9±2.2	8.4±2.4	9.1±2.6
C/D ratio [(ng/ml)/(mg/kg)]	226±154	159±126[a]	201±134	184±167
Month 3				
Daily dose (mg/kg)	0.043±0.024	0.061±0.034[a]	0.046±0.031	0.059±0.024
C_0 (ng/ml)	7.7±2.1	7.0±2.7	7.4±2.2	7.5±2.7
C/D ratio [(ng/ml)/(mg/kg)]	227±131	145±99[a]	209±122	162±127
Month 6				
Daily dose (mg/kg)	0.034±0.019	0.065±0.038[a]	0.042±0.030	0.053±0.032
C_0 (ng/ml)	6.5±2.0	6.4±2.8	6.5±2.3	6.5±2.3
C/D ratio [(ng/ml)/(mg/kg)]	248±132	135±110[a]	216±124	182±157
Month 9				
Daily dose (mg/kg)	0.033±0.018	0.074±0.057[a]	0.045±0.044	0.058±0.038
C_0 (ng/ml)	5.7±2.0	6.6±2.3	5.9±2.1	6.4±2.2
C/D ratio [(ng/ml)/(mg/kg)]	216±162	139±116[a]	191±109	178±154
Month 12				
Daily dose (mg/kg)	0.031±0.019	0.057±0.033[a]	0.037±0.026	0.049±0.030
C_0 (ng/ml)	5.8±1.5	6.3±2.4	6.1±2.0	5.8±1.7
C/D ratio [(ng/ml)/(mg/kg)]	256±178	157±124[a]	239±174	183±149

Data are expressed as the mean±SD.
C_0, trough blood concentration; C/D, dose-adjusted trough blood concentration.
[a]$P<0.05$, significant difference in the mean value from the *CYP3A5*3/*3* group (unpaired *t*-test).

Fig. 5

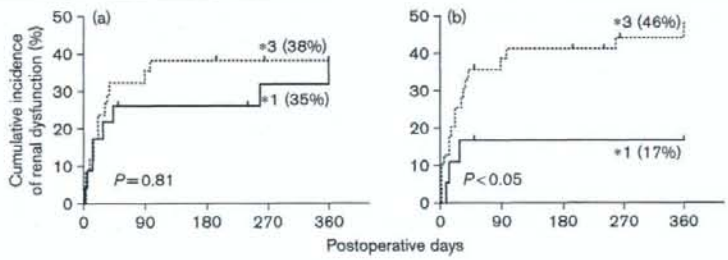

Cumulative incidence of renal dysfunction according to the *CYP3A5* genotypes of donors (a) and recipients (b). Tacrolimus-related nephrotoxicity was defined as an initial increase in the serum creatinine level greater than 0.5 mg/dl above the pretransplant baseline. The solid and dotted curves represent patients carrying the *CYP3A5*1* allele (CYP3A5 expressors, *1) and patients with the *CYP3A5*3/*3* genotype (CYP3A5 nonexpressors, *3), respectively. Small vertical tick marks indicate censored patients (end of follow-up). *P* values were determined with the Kaplan–Meier method and the log-rank test.

studies [13,15–17,19]. As tacrolimus undergoes almost no renal elimination (>95% of dose excreted into bile) [4], indirect mechanisms may be relevant to the inverse correlation between SCR and CL/F. It was reported that tacrolimus clearance increased with time after kidney transplantation [41,42]. From this finding, one possible explanation for the association between SCR and CL/F is that renal failure may result in impaired hepatic metabolism of tacrolimus through the decrease of hepatic CYP3A activity. This mechanism may have occurred in patients who suffered from the hepatorenal syndrome. On the basis of the final model 1 (Table 4), transplant physicians can calculate the tacrolimus dose for an individual patient to achieve the target trough levels early after LDLT, taking renal as well as hepatic function into consideration on each postoperative day.

Limited information is available on the role of enterocyte CYP3A5 in the clinical pharmacokinetics of drugs. Mouly *et al.* [43] studied the pharmacokinetics of saquinavir in

healthy participants and suggested that the increase in the CL/F of saquinavir associated with the *CYP3A5*1* genotype does not reflect intestinal CYP3A5 expression but reflects the contribution of hepatic CYP3A5. Moreover, it has been revealed that patients with a liver graft carrying the *CYP3A5*1* allele had a lower C/D ratio of tacrolimus than patients with a *CYP3A5*3*/**3*-carrying graft liver [10,44,45]. Recently, we have demonstrated that the recovery of tacrolimus CL/F with time after LDLT was increased in pediatric patients with a *CYP3A5*1*-carrying graft liver, but not with the *CYP3A5*1* allele in the native intestine [20]. Interestingly, in this study, adult patients carrying the *CYP3A5*1* allele in the native intestine had a 1.47 times higher (95% CI, 1.17–1.77 times) recovery of tacrolimus CL/F with time than those with the intestinal *CYP3A5*3*/**3* genotype (Fig. 3 and Table 4). These findings were consistent with our previous observation that the tacrolimus C/D ratio was significantly lower in recipients with the intestinal *CYP3A5*1*/**1* genotype than in patients with the *CYP3A5*3*/**3* genotype in enterocytes during the first month after LDLT [11]. One possible explanation for the organ-specific effects of the *CYP3A5*1* genotype on tacrolimus CL/F in pediatric and adult LDLT recipients is the difference in functional graft size between the two populations, who had comparable levels of CYP3A5 mRNA in the native intestine as well as the graft liver at transplantation. Specifically, the native intestine, where CYP3A5 is polymorphically expressed, may more significantly contribute to the first-pass effect of tacrolimus in adult patients receiving a small-for-size graft liver than pediatric patients with an adequate-sized graft.

A significant impact of the intestinal *CYP3A5*1* allele on the individual CL/F estimates was observed during the first 4 weeks of transplant (Fig. 4), which was consistent with our previous results mentioned above [11]. After the first month, the influence of the *CYP3A5*1* genotype in enterocytes was no longer statistically significant (Fig. 4). As shown in Table 5, the intestinal *CYP3A5*1* allele was reported to significantly relate with the increased dose requirements and reduced C/D ratio of tacrolimus on postoperative days 7 and 14 in a univariate analysis, which supports a more important role for enterocyte CYP3A5 in first-pass metabolism than hepatic CYP3A5 immediately after LDLT. The individual Bayesian estimates of CL/F varied widely in patients both with and without the *CYP3A5*1* allele in enterocytes (Fig. 4). To explore the reason for the diversity observed in patients carrying the intestinal *CYP3A5*1* allele (CYP3A5 expressors), we compared the individual CL/F estimates with the mRNA levels of CYP3A5 in the native intestine. No significant correlation, however, was found between them (data not shown). Taking these findings into consideration, the intestinal *CYP3A5*3* polymorphism may be an important determinant for the variability of tacrolimus CL/F in adult LDLT recipients during the first month, although the enterocyte CYP3A5 mRNA level would not predict the interindividual difference in tacrolimus CL/F. Notably, the hepatic but not intestinal *CYP3A5*1* allele significantly influenced tacrolimus dose and C/D ratio throughout the 1-year posttransplant period after the first month (Table 5), suggesting that the major organ influencing tacrolimus disposition changes from the native intestine in the early phase to the graft liver in the stable phase, with the recovery of metabolic function in the liver. From these findings, the impact of enterocyte CYP3A5 on tacrolimus CL/F may be particular to adult LDLT recipients early after surgery, whereas a significant effect of hepatic CYP3A5 on tacrolimus disposition could be a general feature of stable liver transplant patients.

The higher level of MDR1 mRNA in the native intestine led to the significant increase in CL/F (Fig. 3 and Table 4), which was consistent with our previous finding that the initial CL/F was 1.80-fold higher in pediatric LDLT recipients with a high MDR1 mRNA level than those with a low MDR1 mRNA level in enterocytes [20]. These results support the important role of enterocyte P-glycoprotein in the first-pass effect of tacrolimus during the immediate posttransplant period in both pediatric and adult patients receiving LDLT. Taking the intestinal *CYP3A5*1* genotype and MDR1 mRNA level into account, the interindividual variability of CL/F was reduced to 46.2% in the final model 2 from 51.8% in model 1 (Table 4). Consequently, these genotype/phenotype characteristics of adult LDLT recipients could account for approximately 6% of the variation in tacrolimus CL/F. The interindividual and residual variability unexplained in model 2 is still large (Table 4), and may have partly resulted from the concomitant use of inhibitors or inducers of CYP3A and P-glycoprotein such as azole antifungal agents and corticosteroids. A low-dose oral fluconazole (100 mg/day) was used for the prophylaxis of fungal infections in this study. As fluconazole is a less potent inhibitor of CYP3A4 [46], drug–drug interaction between tacrolimus and fluconazole seems not to be responsible for the marked variability in CL/F. The study population included patients receiving intravenous high-dose corticosteroids for the treatment of an acute rejection episode. Corticosteroids have been known to increase tacrolimus clearance, probably by induction of CYP3A4 [4]. Therefore, corticosteroid dose may have contributed to the interindividual variation in the CL/F of tacrolimus.

We previously showed that blood tacrolimus concentrations could be predicted with the Bayesian method 2 weeks after LDLT, when liver function has become stable [47]. Furthermore, our recent study in pediatric LDLT recipients demonstrated that Bayesian forecasting

with the population pharmacokinetic model including genotype/phenotype information provided accurate and less biased predictions of blood tacrolimus concentrations during the first week after surgery [20]. Although the variability of CL/F associated with the intestinal *CYP3A5* genotype and MDR1 mRNA level was relatively small (about 6%), the Bayesian predictions were generally well consistent with the observed concentrations of tacrolimus (Fig. 2b). On the basis of these findings, Bayesian approach-guided dosing with the final model 2 might assist in modifying the maintenance dose of tacrolimus within the early phase as well as the stable phase of transplant. For the care of adult LDLT recipients with the *CYP3A5*1* allele and high MDR1 mRNA levels in enterocytes, a higher dose of tacrolimus should be considered during hospitalization to maintain similar trough concentrations to those in patients with the intestinal *CYP3A5*3/*3* genotype and low MDR1 mRNA levels, owing to the marked difference in tacrolimus CL/F (Fig. 3). Further prospective analysis should be performed to clarify the clinical relevance of a genome-based population pharmacokinetic model for tacrolimus to the reduction of the variability in drug exposure after LDLT.

Interestingly, the cumulative incidence of renal dysfunction over the first year after transplantation was significantly related to the recipient's but not donor's *CYP3A5*1* genotype, whereas similar tacrolimus exposure (C_0) was achieved in expressors and nonexpressors of CYP3A5 (Fig. 5 and Table 5). This result may indicate that CYP3A5 in the kidney plays a protective role in the development of renal dysfunction, probably by reducing exposure of renal cells to tacrolimus. Recently, Kuypers *et al.* [48] suggested that the *CYP3A4*1/CYP3A5*1* and *CYP3A4*1B/CYP3A5*1* genotypes in recipients are associated with the more frequent development of biopsy-proven tacrolimus-related nephrotoxicity within 5 years after kidney transplantation, possibly as a result of higher concentrations of toxic metabolites. They, however, did not examine the potential association with the genotypes in donor kidney. Therefore, we could not clarify the reasons for the discrepancy with the present results. On the basis of our findings, in adult LDLT recipients with the *CYP3A5*3/*3* genotype, the setting of lower target tacrolimus concentrations could lead to less frequent nephrotoxicity, without compromising immunosuppression by introducing or increasing doses of other immunosuppressive drugs such as mycophenolate mofetil. Further studies are needed to investigate renal tissue concentrations as well as nephrotoxicity profiles of tacrolimus and its metabolites such as 13-*O*-desmethyltacrolimus.

In conclusion, we have statistically demonstrated that the MDR1 mRNA level and the *CYP3A5*3* polymorphism in the native intestine contribute to the interindividual difference in the CL/F of tacrolimus in adult patients early after LDLT. In contrast, in the stable phase after transplantation, it is likely that the major organ and molecule that have a significant influence on the tacrolimus CL/F would be changed to hepatic CYP3A5 from intestinal MDR1/CYP3A5. Furthermore, the *CYP3A5*3/*3* genotype in adult LDLT recipients may predispose them to the nephrotoxicity associated with tacrolimus. Understanding these pharmacogenomic properties of tacrolimus will help to establish a more accurate and safe dosage regimen in *de novo* patients receiving LDLT.

Acknowledgements

This study was supported in part by the 21st Century COE Program 'Knowledge Information Infrastructure for Genome Science', by a Grant-in-Aid from the Japan Health Sciences Foundation 'Research on Health Sciences Focusing on Drug Innovation', by a Grant-in-Aid for Scientific Research from the Ministry of Education, Culture, Sports, Science, and Technology of Japan, by a Grant-in-Aid from the Uehara Memorial Foundation, and by a Grant-in-Aid from the Japan Research Foundation for Clinical Pharmacology. K.H. is supported as a Research Assistant by the 21st Century COE Program 'Knowledge Information Infrastructure for Genome Science'.

References

1 Strong RW. Living-donor liver transplantation: an overview. *J Hepatobiliary Pancreat Surg* 2006; **13**:370–377.
2 Todo S, Furukawa H, Jin MB, Shimamura T. Living donor liver transplantation in adults: outcome in Japan. *Liver Transplant* 2000; **6 (Suppl 2)**:66–72.
3 Venkataramanan R, Swaminathan A, Prasad T, Jain A, Zuckerman S, Warty V, *et al.* Clinical pharmacokinetics of tacrolimus. *Clin Pharmacokinet* 1995; **29**:404–430.
4 Staatz CE, Tett SE. Clinical pharmacokinetics and pharmacodynamics of tacrolimus in solid organ transplantation. *Clin Pharmacokinet* 2004; **43**:623–653.
5 Masuda S, Inui K. An up-date review on individualized dosage adjustment of calcineurin inhibitors in organ transplant patients. *Pharmacol Ther* 2006; **112**:184–198.
6 Kahan BD, Keown P, Levy GA, Johnston A. Therapeutic drug monitoring of immunosuppressant drugs in clinical practice. *Clin Ther* 2002; **24**: 330–350.
7 Hebert MF. Contributions of hepatic and intestinal metabolism and P-glycoprotein to cyclosporine and tacrolimus oral drug delivery. *Adv Drug Deliv Rev* 1997; **27**:201–214.
8 Hashida T, Masuda S, Uemoto S, Saito H, Tanaka K, Inui K. Pharmacokinetic and prognostic significance of intestinal MDR1 expression in recipients of living-donor liver transplantation. *Clin Pharmacol Ther* 2001; **69**:308–316.
9 Masuda S, Goto M, Fukatsu S, Uesugi M, Ogura Y, Oike F, *et al.* Intestinal MDR1/ABCB1 level at surgery as a risk factor of acute cellular rejection in living-donor liver transplant patients. *Clin Pharmacol Ther* 2006; **79**: 90–102.
10 Goto M, Masuda S, Kiuchi T, Ogura Y, Oike F, Okuda M, *et al.* CYP3A5*1-carrying graft liver reduces the concentration/oral dose ratio of tacrolimus in recipients of living-donor liver transplantation. *Pharmacogenetics* 2004; **14**:471–478.
11 Uesugi M, Masuda S, Katsura T, Oike F, Takada Y, Inui K. Effect of intestinal CYP3A5 on postoperative tacrolimus trough levels in living-donor liver transplant recipients. *Pharmacogenet Genomics* 2006; **16**:119–127.
12 Sam WJ, Aw M, Quak SH, Lim SM, Charles BG, Chan SY, *et al.* Population pharmacokinetics of tacrolimus in Asian paediatric liver transplant patients. *Br J Clin Pharmacol* 2000; **50**:531–541.
13 García Sánchez MJ, Manzanares C, Santos-Buelga D, Blázquez A, Manzanares J, Urruzuno P, *et al.* Covariate effects on the apparent clearance

of tacrolimus in paediatric liver transplant patients undergoing conversion therapy. *Clin Pharmacokinet* 2001; **40**:63–71.
14 Staatz CE, Taylor PJ, Lynch SV, Willis C, Charles BG, Tett SE. Population pharmacokinetics of tacrolimus in children who receive cut-down or full liver transplants. *Transplantation* 2001; **72**:1056–1061.
15 Antignac M, Hulot JS, Boleslawski E, Hannoun L, Touitou Y, Farinotti R, *et al.* Population pharmacokinetics of tacrolimus in full liver transplant patients: modelling of the post-operative clearance. *Eur J Clin Pharmacol* 2005; **61**:409–416.
16 Zahir H, McLachlan AJ, Nelson A, McCaughan G, Gleeson M, Akhlaghi F. Population pharmacokinetic estimation of tacrolimus apparent clearance in adult liver transplant recipients. *Ther Drug Monit* 2005; **27**:422–430.
17 Lee JY, Hahn HJ, Son IJ, Suh KS, Yi NJ, Oh JM, *et al.* Factors affecting the apparent clearance of tacrolimus in Korean adult liver transplant recipients. *Pharmacotherapy* 2006; **26**:1069–1077.
18 Yasuhara M, Hashida T, Toraguchi M, Hashimoto Y, Kimura M, Inui K, *et al.* Pharmacokinetics and pharmacodynamics of FK 506 in pediatric patients receiving living-related donor liver transplantations. *Transplant Proc* 1995; **27**:1108–1110.
19 Fukatsu S, Yano I, Igarashi T, Hashida T, Takayanagi K, Saito H, *et al.* Population pharmacokinetics of tacrolimus in adult recipients receiving living-donor liver transplantation. *Eur J Clin Pharmacol* 2001; **57**: 479–484.
20 Fukudo M, Yano I, Masuda S, Goto M, Uesugi M, Katsura T, *et al.* Population pharmacokinetic and pharmacogenomic analysis of tacrolimus in pediatric living-donor liver transplant recipients. *Clin Pharmacol Ther* 2006; **80**: 331–345.
21 Kiuchi T, Kasahara M, Uryuhara K, Inomata Y, Uemoto S, Asonuma K, *et al.* Impact of graft size mismatching on graft prognosis in liver transplantation from living donors. *Transplantation* 1999; **67**:321–327.
22 Sugawara Y, Makuuchi M, Takayama T, Imamura H, Dowaki S, Mizuta K, *et al.* Small-for-size grafts in living-related liver transplantation. *J Am Coll Surg* 2001; **192**:510–513.
23 Mochizuki N, Matsumoto K, Ohno K, Shimamura T, Furukawa H, Todo S, *et al.* Effects of hepatic CYP3A4 activity on disposition of micafungin in liver transplant recipients with markedly small-for-size grafts. *Transplant Proc* 2006; **38**:3649–3650.
24 Kishino S, Ohno K, Shimamura T, Furukawa H, Todo S. A nomogram for predicting the optimal oral dosage of tacrolimus in liver transplant recipients with small-for-size grafts. *Clin Transplant* 2006; **20**:443–449.
25 Ojo AO, Held PJ, Port FK, Wolfe RA, Leichtman AB, Young EW, *et al.* Chronic renal failure after transplantation of a nonrenal organ. *N Engl J Med* 2003; **349**:931–940.
26 Hebert MF, Dowling AL, Gierwatowski C, Lin YS, Edwards KL, Davis CL, *et al.* Association between ABCB1 (multidrug resistance transporter) genotype and post-liver transplantation renal dysfunction in patients receiving calcineurin inhibitors. *Pharmocogenetics* 2003; **13**:661–674.
27 Hauser IA, Schaeffeler E, Gauer S, Scheuermann EH, Wegner B, Gossmann J, *et al.* ABCB1 genotype of the donor but not of the recipient is a major risk factor for cyclosporine-related nephrotoxicity after renal transplantation. *J Am Soc Nephrol* 2005; **16**:1501–1511.
28 Dai Y, Iwanaga K, Lin YS, Hebert MF, Davis CL, Huang W, *et al. In vitro* metabolism of cyclosporine A by human kidney CYP3A5. *Biochem Pharmacol* 2004; **68**:1889–1902.
29 Dai Y, Hebert MF, Isoherranen N, Davis CL, Marsh C, Shen DD, *et al.* Effect of CYP3A5 polymorphism on tacrolimus metabolic clearance *in vitro*. *Drug Metab Dispos* 2006; **34**:836–847.
30 Joy MS, Hogan SL, Thompson BD, Finn WF, Nickeleit V. Cytochrome P450 3A5 expression in the kidneys of patients with calcineurin inhibitor nephrotoxicity. *Nephrol Dial Transplant* 2007; **22**:1963–1968.
31 Cogill JL, Taylor PJ, Westley IS, Morris RG, Lynch SV, Johnson AG. Evaluation of the tacrolimus II microparticle enzyme immunoassay (MEIA II) in liver and renal transplant recipients. *Clin Chem* 1998; **44**:1942–1946.
32 Goto M, Masuda S, Saito H, Uemoto S, Kiuchi T, Tanaka K, *et al.* C3435T polymorphism in the MDR1 gene affects the enterocyte expression level of CYP3A4 rather than Pgp in recipients of living-donor liver transplantation. *Pharmacogenetics* 2002; **12**:451–457.
33 Chowbay B, Cumaraswamy S, Cheung YB, Zhou Q, Lee EJ. Genetic polymorphisms in MDR1 and CYP3A4 genes in Asians and the influence of MDR1 haplotypes on cyclosporin disposition in heart transplant recipients. *Pharmacogenetics* 2003; **13**:89–95.
34 Kuehl P, Zhang J, Lin Y, Lamba J, Assem M, Schuetz J, *et al.* Sequence diversity in CYP3A promoters and characterization of the genetic basis of polymorphic CYP3A5 expression. *Nat Genet* 2001; **27**:383–391.
35 Saeki M, Saito Y, Nakamura T, Murayama N, Kim SR, Ozawa S, *et al.* Single nucleotide polymorphisms and haplotype frequencies of CYP3A5 in a Japanese population. *Hum Mutat* 2003; **21**:653.
36 Beal SL, Boeckmann AJ, Sheiner LB. *NONMEM users guides*. San Francisco: NONMEM Project Group, University of California at San Francisco; 1992.
37 Kirchheiner J, Bauer S, Meineke I, Rohde W, Prang V, Meisel C, *et al.* Impact of CYP2C9 and CYP2C19 polymorphisms on tolbutamide kinetics and the insulin and glucose response in healthy volunteers. *Pharmacogenetics* 2002; **12**:101–109.
38 Yates CR, Zhang W, Song P, Li S, Gaber AO, Kotb M, *et al.* The effect of CYP3A5 and MDR1 polymorphic expression on cyclosporine oral disposition in renal transplant patients. *J Clin Pharmacol* 2003; **43**: 555–564.
39 Hesselink DA, van Gelder T, van Schaik RH, Balk AH, van der Heiden IP, van Dam T, *et al.* Population pharmacokinetics of cyclosporine in kidney and heart transplant recipients and the influence of ethnicity and genetic polymorphisms in the MDR-1, CYP3A4, and CYP3A5 genes. *Clin Pharmacol Ther* 2004; **76**:545–556.
40 Djebli N, Rousseau A, Hoizey G, Rerolle JP, Toupance O, Le Meur Y, *et al.* Sirolimus population pharmacokinetic/pharmacogenetic analysis and bayesian modelling in kidney transplant recipients. *Clin Pharmacokinet* 2006; **45**:1135–1148.
41 Aweeka FT, Benet LZ, Gambertoglio JG, Peter K, Okudaira N, Kinda J, *et al.* Comparative pharmacokinetics of orally (PO) and intravenously (IV) administered tacrolimus (FK506) in pre- and post-kidney transplant recipients. *Clin Pharmacol Ther* 1993; **53**:151.
42 Antignac M, Barrou B, Farinotti R, Lechat P, Urien S. Population pharmacokinetics and bioavailability of tacrolimus in kidney transplant patients. *Br J Clin Pharmacol* 2007; **64**:750–757.
43 Mouly SJ, Matheny C, Paine MF, Smith G, Lamba J, Lamba V, *et al.* Variation in oral clearance of saquinavir is predicted by CYP3A5*1 genotype but not by enterocyte content of cytochrome P450 3A5. *Clin Pharmacol Ther* 2005; **78**:605–618.
44 Yu S, Wu L, Jin J, Yan S, Jiamg G, Xie H, *et al.* Influence of CYP3A5 gene polymorphisms of donor rather than recipient to tacrolimus individual dose requirement in liver transplantation. *Transplantation* 2006; **81**:46–51.
45 Wei-lin W, Jing J, Shu-sen Z, Li-hua W, Ting-bo L, Song-feng Y, *et al.* Tacrolimus dose requirement in relation to donor and recipient ABCB1 and CYP3A5 gene polymorphisms in Chinese liver transplant patients. *Liver Transplant* 2006; **12**:775–780.
46 Venkatakrishnan K, von Moltke LL, Greenblatt DJ. Effects of the antifungal agents on oxidative drug metabolism: clinical relevance. *Clin Pharmacokinet* 2000; **38**:111–180.
47 Fukudo M, Yano I, Fukatsu S, Saito H, Uemoto S, Kiuchi T, *et al.* Forecasting of blood tacrolimus concentrations based on the Bayesian method in adult patients receiving living-donor liver transplantation. *Clin Pharmacokinet* 2003; **42**:1161–1178.
48 Kuypers DR, de Jonge H, Naesens M, Lerut E, Verbeke K, Vanrenterghem Y. CYP3A5 and CYP3A4 but not MDR1 single-nucleotide polymorphisms determine long-term tacrolimus disposition and drug-related nephrotoxicity in renal recipients. *Clin Pharmacol Ther* 2007; **82**:711–725.

Journal of Cellular Physiology

A Model for Diabetic Nephropathy: Advantages of the Inducible cAMP Early Repressor Transgenic Mouse Over the Streptozotocin-Induced Diabetic Mouse

AKARI INADA,[1,2] HIROSHI KANAMORI,[3] HIDENORI ARAI,[4]* TOMOYUKI AKASHI,[2] MAKOTO ARAKI,[3] GORDON C. WEIR,[2] AND ATSUSHI FUKATSU[3]

[1] *SSP Stem Cell Unit, Kyushu University Graduate School of Medicine, Fukuoka, Japan*

[2] *Islet Transplantation and Cell Biology, Joslin Diabetes Center, Boston, MA*

[3] *Department of Nephrology, Kyoto University Graduate School of Medicine, Kyoto, Japan*

[4] *Department of Geriatric Medicine, Kyoto University Graduate School of Medicine, Kyoto, Japan*

We have previously found progressive diabetic nephropathy in inducible cAMP early repressor (ICER Iγ) transgenic (Tg) mice. The ICER Iγ Tg mouse is an interesting model of sustained hyperglycemia due to its low production of insulin and insulin-producing β cells. Here in a longitudinal study we further analyzed diabetic nephropathy and structural and functional alterations in other organs, comparing our model with streptozotocin (STZ)-diabetic model mice. The high-dose STZ-diabetic model showed marked variation in blood glucose levels and severe toxicity of STZ in the liver and kidney. The low-dose STZ-diabetic model showed less toxicity, but the survival rate was very low. STZ-diabetic mice had much more variation of glomerular hypertrophy and sclerosis. Furthermore, non-specific toxicity of STZ or insulin injections to maintain optimal blood glucose levels might have another effect upon the diabetic renal changes. In contrast, ICER Iγ Tg mice exhibited a stable and progressive phenotype of diabetic kidney disease solely due to chronic hyperglycemia without other modulating factors. Thus, ICER Iγ Tg mouse has advantages for examining diabetic renal disease, and offers unique and very different perspectives compared to STZ model.

J. Cell. Physiol. 215: 383–391, 2008. © 2008 Wiley-Liss, Inc.

Biomedical experiments in mice provide significant advantages for studying mammalian diseases since inbred mice have a uniform genetic background. To investigate the pathogenesis of diabetic nephropathy, appropriate animal models are required. Although numerous animal models have been established in rodents (Breyer et al., 2005), these diabetic animals develop limited or only mild kidney disease that resembles human diabetic nephropathy (Tochino, 1987; Williamson et al., 1987; Doi et al., 1990; Janssen et al., 2003), and no single animal model that develops renal changes identical to those seen in humans has been developed (Velasquez et al., 1990).

So far the streptozotocin (STZ)-induced diabetic mouse model is commonly used. STZ-induced DNA damage leads to reduction of the cellular ATP content and then death of pancreatic β cells (Szkudelski, 2001). Low-dose STZ elicits non-specific islet inflammation with infiltrating mononuclear cells (Like and Rossini, 1976; Like et al., 1978). High-dose single injections of STZ cause β-cell necrosis within 2–4 h (Junod et al., 1967) with rapid clearance of STZ (Schein et al., 1973). Because neonatal STZ-treatment has oncogenic effects on liver, kidney, and pancreas (Iwase et al., 1989), adult animals are used for induction of diabetes. However, there are several problems in this model: (I) STZ is harmful and carcinogenic for animals (Like and Rossini, 1976; Like et al., 1978), and induces toxicity in multiple organs (Nukatsuka et al., 1990; Sotnikova et al., 1999; Wang et al., 2000; Imaeda et al., 2002; Koulmanda et al., 2003; Brondum et al., 2005). STZ is taken up by a glucose transporter into renal proximal tubular cells to induce tubular alterations (Sadoff, 1970; Tay et al., 2005). High-dose STZ directly damages and alters the renal function during the first week after STZ injection. In addition, STZ affects not only renal excretion of electrolytes and protein, but also renal microcirculation and oxygen metabolism (Palm et al., 2004). Therefore, the renal damage in STZ mice is induced not only by hyperglycemia but by

Contract grant sponsor: Scientific Research, Ministry of Education, Culture, Sports, Science and Technology;
Contract grant number: 19890150.
Contract grant sponsor: Creative Scientific Research, Ministry of Education, Culture, Sports, Science and Technology;
Contract grant number: NP10NPO201.
Contract grant sponsor: Japan Society for the Promotion of Science;
Contract grant number: JSPS-RFTF97100201.
Contract grant sponsor: Japan Diabetes Foundation.
Contract grant sponsor: Mochida Memorial foundation.

Akari Inada's present address is SSP Stem Cell Unit, Kyushu University Graduate School of Medicine, 3-1-1 Maidashi, Higashi-ku, Fukuoka 812-8582, Japan.

*Correspondence to: Hidenori Arai, Department of Geriatric Medicine, Kyoto University Graduate School of Medicine, 54 Kawahara-cho, Shogoin, Sakyo-ku, Kyoto 606-8507, Japan. E-mail: harai@kuhp.kyoto-u.ac.jp

Received 27 August 2007; Accepted 11 September 2007

DOI: 10.1002/jcp.21316

© 2008 WILEY-LISS, INC.

STZ itself (Churchill et al., 1993; Lee et al., 1974). (II) To maintain optimal blood glucose levels for survival, daily insulin injections are often required, and it is difficult to maintain optimal glucose levels. Insulin might have additional effects on diabetic renal changes. (III) STZ is not sufficient for a useful model of progressive renal disease. STZ mice show mesangial expansion, but they show glomerulosclerosis only in limited backgrounds (Breyer et al., 2005, 2006). STZ plus subtotal nephrectomy (Yokozawa et al., 2001) or STZ plus high protein diet (Zatz et al., 1985) has been used to accelerate the process. (IV) In STZ mice, much more variation of renal lesions is observed, which makes it difficult to evaluate the nephropathy correctly and requires a large number of mice for proper statistical analysis of the renal disease.

We previously developed a severe diabetic mouse model, inducible cAMP early repressor (ICER Iγ) transgenic (Tg) mice (Inada et al., 2004). ICER Iγ is a transcriptional repressor transcribed from an alternative intronic promoter of the *CREM* gene and consists of only a DNA-binding domain (Foulkes et al., 1991; Inada et al., 1998). ICER Iγ competes with transcriptional activators for binding to the DNA, and strongly represses insulin (Inada et al., 1999) and cyclin A (Inada et al., 2005a) gene transcription. In this mouse, ICER Iγ is overexpressed only in pancreatic β cells, not in other organs (Inada et al., 2004). The suppression of insulin synthesis and β cell proliferation results in severe diabetes as early as 2 weeks of age (Inada et al., 2004). Hyperglycemia is sustained by 40 weeks of age, but mice show an excellent survival rate without insulin therapy (Inada et al., 2004). In this model, we have found that the diabetic renal change starts with glomerular hypertrophy, followed by glomerular basement membrane (GBM) thickening and development of sclerotic lesions, thus mimicking the progression of human diabetic nephropathy (Inada et al., 2005b).

Here, in a longitudinal study, we further analyzed diabetic nephropathy and functional and morphological alterations of other organs (liver and pancreas), comparing our model with STZ mice. Our model offers a unique and very different perspective of diabetic nephropathy compared to STZ-diabetic mice.

Materials and Methods

Generation of ICER Iγ Tg mice

ICER Iγ transgenic (ICER Tg) mice were made as described previously (Inada et al., 2004). Their background strain is C57BL/6J (Japan SLC, Inc., Hamamatsu, Shizuoka, Japan). Three transgenic lines (Tg 7, Tg 12, Tg 23) were obtained from 62 founder mice. Copy numbers of the transgene in founder mice were 4, 4, and 6, respectively, determined by Southern blot analysis. Tg mice were identified by PCR analysis of tail DNA. In all experiments, non-transgenic littermates (wild type, WT) were used as controls. Mice were housed in microisolator cages in a temperature-controlled room at 24 ± 2°C and at 50 ± 10% relative humidity under 12-h light/dark cycle. Standard rodent diet (CE-2; CLEA Japan, Inc., Tokyo, Japan) and water were supplied ad libitum. All mice were handled in accordance with the Guidelines for Animal Experiments of Kyoto University. The data presented here are from F2 to F4 males only of line Tg 23.

STZ-induced diabetic model mouse

Weight-matched 8-week-old male mice (C57BL/6J) were treated with STZ (Sigma Chemical Co., St. Louis, MO) or sterile citrate buffer (pH 4.5) alone, according to the animal models of diabetic complications consortium (AMDCC) protocol. STZ was freshly dissolved in sterile citrate buffer (pH 4.5) and injected intraperitoneally into mice (50, 150, or 200 mg/kg). Mice treated with 50 mg/kg of STZ (STZ-50) were fasted for 4-h prior to STZ induction, and were given one injection for 5 days consecutively. Mice treated with 150 or 200 mg/kg of STZ (STZ-150 or -200) were given a single i.p. injection of STZ. Only mice with blood glucose concentrations greater than 400 mg/dl in the fed state were used as diabetic in the experiments for each group.

Histological study

ICER Tg, STZ and control (N = 6 for each group) mouse kidney, pancreases, and livers were fixed in methyl Carnoy's solution or 10% buffered formalin, embedded in paraffin, and cut in serial sections (2 μm). Kidney sections were stained with periodic acid-Schiff (PAS) and periodic acid-methenamine silver (PASM). Liver and pancreas sections were stained with hematoxylin and eosin (H&E) using standard histological procedures.

Measurements of glomerular surface area and PASM-positive area. PASM-positive area and glomerular surface area were measured in PASM stained sections using Image-Pro Plus (Media Cybernetics, Silver Spring, MD). For each mouse, 50 glomeruli were analyzed. PASM-positive area fraction was calculated as the ratio of PASM-positive area to glomerular surface area (Nagai et al., 2003).

Immunohistochemistry

Mouse pancreases were fixed in 10% buffered formalin, embedded in paraffin, and cut in serial sections (2 μm). For immunohistochemistry, primary antibodies, anti-insulin (1:500; DAKO), anti-ICER (anti-serum α-CREM S4; 1:500; kindly provided J. F. Habener, Maassachusetts General Hospital, Howard Hughes Medical Institute), and anti-glucagon (1:3,000; Linco Reasearch, Inc., St. Charles, MO) were used. Primary antibody was detected by immunofluorescence labeling with FITC-conjugated or Texas red-conjugated secondary antibodies or by imunoperoxidase with biotin-labeled secondary antibody. Staining was visualized with diaminobenzidine.

Measurements of serum variables

Blood glucose levels were determined by an enzyme-electrode method using GLUTEST (Sanwa Kagaku, Nagoya, Japan) on whole blood taken from the tail vein. For other parameters, blood was withdrawn from the heart immediately before isolation of the kidney under pentobarbital anesthesia. Creatinine was measured by HPLC. Total cholesterol was measured by enzymatic assays (Wako Pure Chemical Industries Ltd., Kyoto, Japan). Albumin was measured by BCG method (SRL, Inc., Tokyo, Japan).

Measurements of urinary variables

The urinary parameters measured were albumin and creatinine. They were measured at 8–40 weeks of age in 24-h urine collection samples from mice housed in individual metabolic cages (N = 6 in each group). During the urine collection, mice were allowed free access to food and water. Albumin concentration was assayed using the Albuwell kit (Exocell, Inc., Philadelphia, PA). Creatinine was measured by HPLC as described above. Body-weight adjusted creatinine clearance (Ccr) was calculated by the following equation: Ccr = urine creatinine (mg/dl) × urine volume (μl/min)/serum creatinine (mg/dl)/body weight (g) (Nagasao et al., 2005).

Data analysis

Data are presented as mean ± SD. Comparison among each group was performed by one-way analysis of variance (ANOVA) followed by Neuman–Keuls test to evaluate statistical significance between two groups. For multiple comparison and changes in blood glucose levels, repeated measure ANOVA, Kruskal–Wallis test, and post hoc Bonferroni/Dunn test were used. A *P*-value less than 0.05 was considered statistically significant.

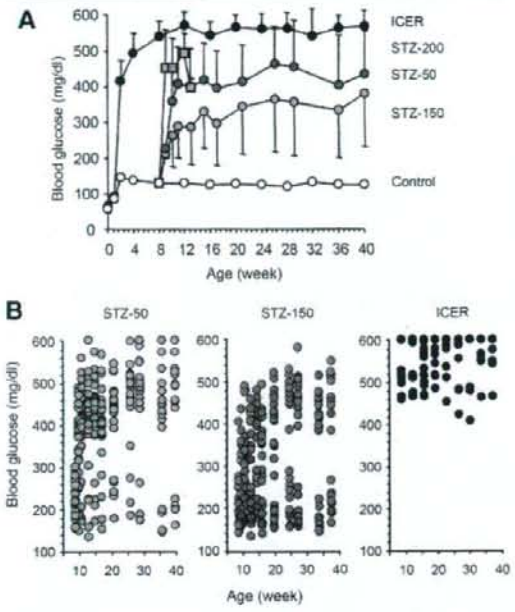

Fig. 1. ICER Tg mice exhibited sustainable hyperglycemia. A: Fed blood glucose levels at indicated weeks. The three dose of STZ (50 or 150 or 200 mg/kg) were injected intraperitoneally into male mice at 8 weeks of age. Fed blood glucose levels of STZ-200 mice (light-gray square) elevated very fast, and they died within 4–8 weeks of injection. Increase of fed blood glucose levels of STZ-50 mice (dark-gray circle) and STZ-150 mice (light-gray circle) were more gradual but unstable. In ICER Tg mice (black circle) severe hyperglycemia was sustained. Results are expressed as mean ± SD. B: In STZ-diabetic mice, there is a marked variation of fed blood glucose levels. N = 24 for each STZ-diabetic group, N = 14 for ICER Tg mice. Each circle represents an animal, but some circles represent 5–9 animals since they had same blood glucose levels (black circle in ICER Tg mice).

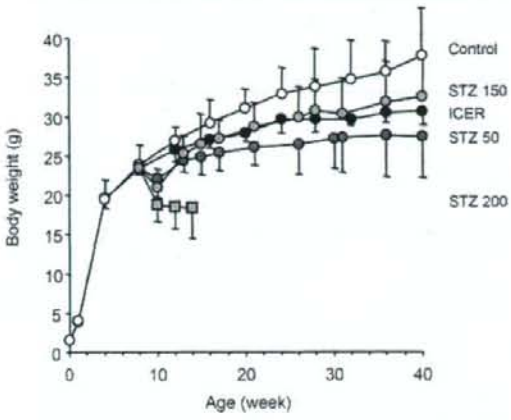

Fig. 2. Body weight of male mice. The growth curve of male mice from day 0 to 40 weeks of age is shown. STZ-200 mice (light-gray square) lost body weight and died soon. Results are expressed as mean ± SD. N = 24 for each STZ-diabetic group, N = 14 for ICER Tg mice.

Results

ICER Tg mice exhibit sustained hyperglycemia

In ICER Tg mice, blood glucose levels were normal at birth, but became markedly increased by 2 weeks of age, and severe hyperglycemia was sustained at least until 40 weeks of age (Fig. 1A). These mice survived well without insulin therapy, and had no obesity or severe emaciation. In STZ-50 and STZ-150 mice, following injection of STZ, blood glucose levels became gradually hyperglycemic within 3 weeks, and increased until 26 weeks of age. In addition, there was a marked variation of fed blood glucose levels in STZ mice (Fig. 1B). STZ-200 mice developed severe diabetes soon after the STZ injection (Fig. 1A), with a sharp drop in body weight (Fig. 2), which led to death within 4–8 weeks of injection.

In ICER Tg mice, body weight was similar to that of controls until 8 weeks of age, but they failed to gain weight thereafter (Fig. 2). STZ-150 mice showed a similar body weight change to ICER Tg mice, but started to gain weight after 30 weeks of age. Body weight of STZ-50 mice was lower than that of ICER Tg mice at all time points during the study, with only a slight increase after STZ injection.

Eleven out of 24 diabetic STZ-50 mice survived for the entire 40 weeks. Soon after 40 weeks three more mice died. In contrast, the survival rate of ICER Tg mice was excellent; 12 of 14 ICER Tg mice survived.

Islet morphology

STZ causes preferential death of pancreatic β cells by its uptake in these cells via GLUT-2 glucose transporter. Because there are few insulin-positive cells left in islets, pancreatic sections from 40-week old mice were immunostained for glucagon. In controls, the typical islet morphology of a mantle of glucagon-positive cells (brown) was seen (Fig. 3A, left). In contrast, in STZ-150 mice, the islets appeared severely disorganized with an increased proportion of glucagon-positive cells (Fig. 3A, middle). In STZ-50 mice, there was a marked variation in islet size and the number of β cells in the islet as shown in Figure 3B. The islet morphology in STZ mice was similar to that of ICER Tg mice. In ICER Tg mice, insulin-positive cells (green) are reduced due to ICER expression (red) (Fig. 3C), so the islets appear severely disorganized with a significantly increased proportion of glucagon-positive cells (Fig. 3A, right). Thus, serum insulin levels were extremely low (12 weeks, line Tg23 male Tg mice vs. control male mice, 278 ± 111 vs. 1,350 ± 195 pg/ml, $P < 0.001$).

Liver toxicity of STZ

The liver toxicity was examined by measuring organ weights and serum aspartate aminotransfase (AST) and alanine aminotransfase (ALT) levels. There was no significant difference in liver weight (Fig. 4A), but liver weight/body weight in STZ-diabetic mice was higher than that in ICER Tg mice at 40 weeks of age (Fig. 4B). ICER liver weight/body weight was probably a little high due to modest body weight decrease from controls. The ratio of AST/ ALT was significantly increased in STZ-diabetic mice group (Fig. 4C). The liver section showed severe hepatic steatosis in STZ-diabetic mice (Fig. 5).

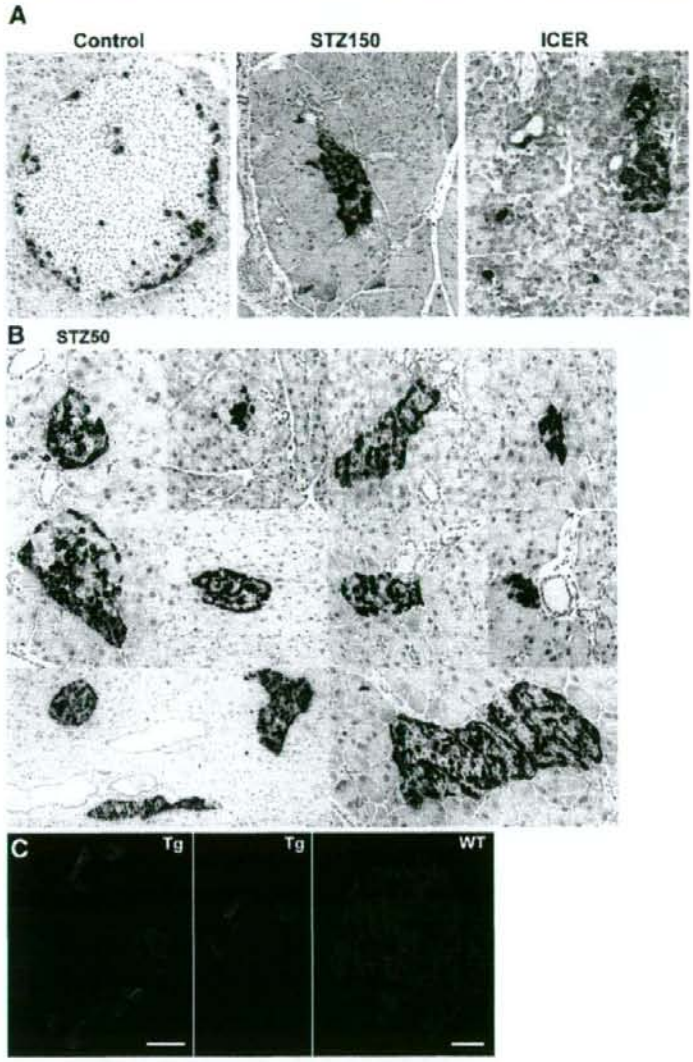

Fig. 3. Islet morphology. Glucagon staining of pancreatic sections of 40 week-old-mice. A: In STZ-150 mice and ICER Tg mice, islets appear severely disorganized with a significantly increased proportion of glucagon-positive (brown) cells. B: In STZ-50 mice there is a variation in the size as shown by the glucagon staining. The non-stained cells present as aggregating in the middle of the islets are assumed to be β cells. Magnification, 200× (A–D) and 100× (D, left low panel only). C: Reduced insulin synthesis and β-cell numbers in a representative islet. Dual staining of pancreatic sections with anti-insulin (green) and anti-ICER (red) antibody was analyzed by confocal microscopy.

Diabetic nephropathy

Glomerular hypertrophy and subsequent glomerulosclerosis are the characteristic histological findings lesions in diabetic nephropathy. To analyze the hypertrophy and glomerulosclerosis, we measured glomerular surface area and PASM-positive areas. Renal glomerular sclerotic lesions seen in STZ nice are variable and they were milder (Fig. 6A,B), whereas lesions in Tg mice were more severe and constant (Fig. 6C). There was a significant difference in PASM-positive areas between STZ-150 mice and ICER Tg mice ($P = 0.014$) (Fig. 6D).

Renal functional measurement

Clearance studies are some of the most valuable means of determining the stage of nephropathy, with Ccr, a reliable test to measure GFR. In both STZ-diabetic mice and ICER Tg mice, Ccr was significantly higher at 40 weeks of age than in controls

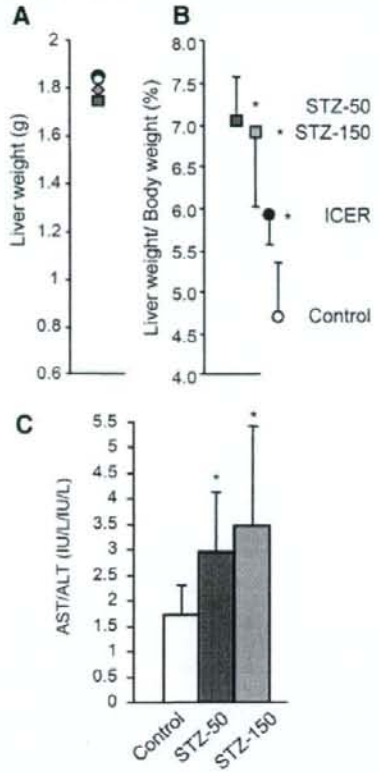

Fig. 4. The damage of the liver in STZ-diabetic mice. A: Liver weight. B: Liver weight/ body weight of STZ-diabetic mice at 40 weeks of age was elevated, since they had lower body weight. C: The AST/ALT ratio was significantly increased in STZ-diabetic mice. Results are expressed as mean ± SD. N = 6 for each group.

(Fig. 7A,B). In ICER Tg mice, the peak of Ccr was at 20 weeks of age, and then decreased toward 40 weeks of age. There was no significant difference in serum creatinine at 40 weeks of age (Fig. 7C). We also examined kidney weights. Renal hypertrophy was expressed as the ratio of the total kidney weight (the combined weight of the two kidneys) to body weight. In ICER Tg mice, the kidney weight increased with age (Fig. 7D), and renal hypertrophy was also prominent (Fig. 7E), which started at 8 weeks of age. In contrast, in STZ mice the kidney weight was not increased and showed no significant difference from controls (Fig. 7D). Renal hypertrophy was seen in STZ mice, but less than that in ICER Tg mice at 40 weeks of age (Fig. 7E). The urinary albumin excretion rates in both ICER Tg mice and STZ mice were higher at 40 weeks of age than in control mice (Fig. 8A). At the same time, serum albumin was significantly lower (Fig. 8B) and urine volume and total cholesterol were higher in both ICER Tg mice and STZ-diabetic mice than in control mice (Fig. 8C,D).

Discussion

In this longitudinal study, we assessed diabetic nephropathy and structural and functional alterations in organs in ICER Tg mouse

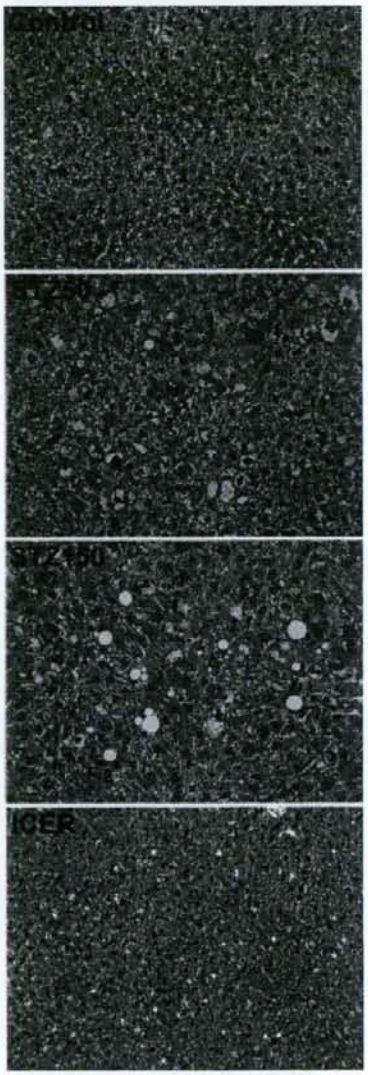

Fig. 5. Liver morphology. Hematoxylin and eosin (H&E) staining at 40-week-old mice. STZ-150 mice show marked steatosis and cholestasis. Magnification, 200×.

and compared them with corresponding changes in STZ-induced diabetic mice. To assess the toxicity of this diabetologenic agent to organs, we used high- and low-dose STZ according to the AMCC protocol.

First, we assessed the pancreatic morphology in these models. Although single injections of high-dose STZ show marked variation in blood glucose levels, and are toxic to other organs (Sotnikova et al., 1999; Koulmanda et al., 2003), we consistently observed irreversible and complete destruction of β cells in diabetic STZ-150 mice. On the other hand, low-dose

STZ with multiple injections damages β cells more slowly within 12 h of STZ-treatment (Nagasao et al., 2005) with lower toxicity to other organs (Koulmanda et al., 2003), but it causes a variation in the degree of β-cell death, this leaving some residual β cells in STZ-50 mice. Susceptibility to the low-dose STZ appeared to be somewhat different in each animal, and more than half of the mice could not survive for the entire 40 weeks. Thus, destroying β cells by giving a chemical compound seems to cause varying levels of β-cell death, blood glucose levels, and survival. Since blood glucose levels and the diabetic period greatly affect the development of diabetic nephropathy, it was hard to produce stable renal changes in a sufficient number of STZ mice in this longitudinal study.

In contrast, in ICER Tg mice, both insulin synthesis and β-cell proliferation are suppressed genetically by overexpression of ICER Iγ. Insulin synthesis is substantially repressed at the transcriptional level from the fetal period. Normally the burst of β-cell replication after birth is important to expand β-cell population to produce enough insulin (Bonner-Weir, 2000). In ICER Tg mice, however, β-cell proliferation is limited through reduced cyclin A expression, which is required for normal cell cycle progression. Limitation of β-cell proliferation reduces not only β-cell number within islets but also insulin production. Therefore, ICER Tg mice uniformly lose β cells with time but retain a small number, which accounts for the maintenance of stable hyperglycemia.

In STZ-injected animals, complications include toxicity of aorta (Sotnikova et al., 1999), arteries (Brondum et al., 2005), liver, and kidney (Koulmanda et al., 2003); DNA damage in these tissues is well studied (Wang et al., 2000; Imaeda et al., 2000). In the STZ liver and kidney, DNA synthesis and tissue repair responses are delayed (Wang et al., 2000), oxygen consumption of mitochondria is decreased in a time- and dose-dependent manner (Nukatsuka et al., 1990), which increases necrosis from 12 h onward and progresses (Wang et al., 2000). Although DNA damage in the liver and kidney recovers slowly with time (Imaeda et al., 2002), we still found injury in these organs in STZ mice at 40 weeks of age. Elevated AST/ALT ratio and severe hepatic steatosis showed that liver was both functionally and morphologically damaged.

It is well known that hyperglycemia induces formation of reactive oxygen species (ROS), and that ROS, transforming growth factor-β1 (TGF-β1), and hypertension enhance the progression of diabetic nephropathy (Palm, 2006; Tesch and Nikolic-Paterson, 2006; Lee et al., 2007; Tojo et al., 2007). It has been also reported that the oxidative stress is mainly associated with hypertension in diabetic renal injury, and not associated as strongly with hyperglycemia (Tomohiro et al., 2007). We have measured systolic blood pressure (SBP) using tail-cuff method at 20 weeks of age. SBP in the ICER Tg mouse group was slightly higher than that in WT mouse group (Tg vs. WT, 113.1 ± 0.8 vs. 96.4 ± 0.8 mmHg, $P < 0.01$). Therefore, in ICER Tg mice it is possible that ROS are produced by sustained hyperglycemia, and oxidative stress could be associated with hypertension. Since it seems complex, further study is needed to find a factor playing a major role in progression of diabetic nephropathy in this model.

There are four advantages of ICER Tg mice compared to STZ mice: (1) ICER Tg mice stably develop hyperglycemia and renal changes. Hyperglycemia develops at about 2 weeks of age and continues throughout life, and these mice show excellent survival. Since each mouse has almost identical diabetic renal

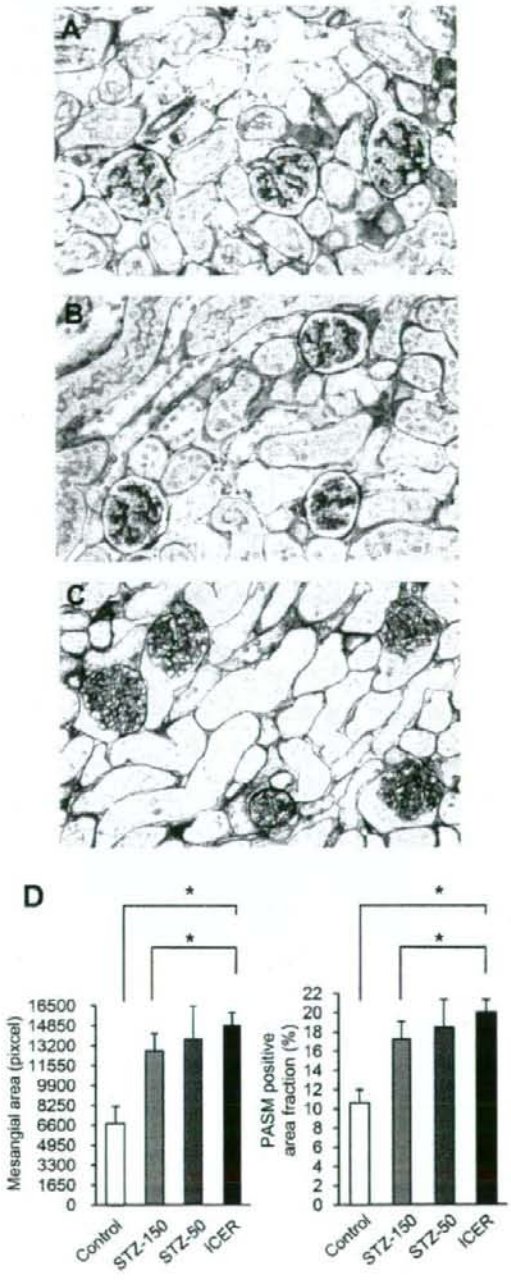

Fig. 6. Diabetic nephropathy. A–C: Representative glomeruli from 40-week-old mice. Renal glomerular sclerotic lesions seen in STZ nice are variable and they were milder (A,B), whereas lesions in Tg mice were more severe and constant (C). D: PASM-positive area was measured by image-Pro Plus in 50 glomeruli for each mouse. PASM-positive area fraction was calculated by the ratio of PASM-positive area to total glomerular surface area. Data are mean ± SD. N = 6 per each group. Kidney sections were stained with PASM. Magnification, 200×.

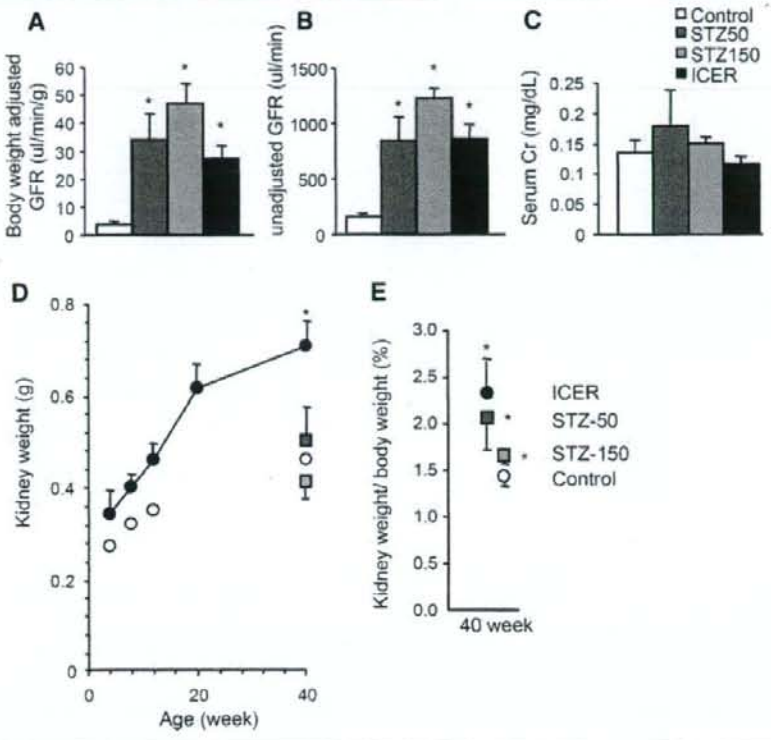

Fig. 7. Hemodynamic change in STZ-diabetic and ICER Tg mice. A,B: The glomerular filtration rate (GFR) was calculated as described in Materials and Methods Section. C: Serum creatinine was measured by HPLC. D: Kidney weight curve in ICER Tg mice (black circle) from 4 to 40 weeks of age and kidney weight in STZ-diabetic mice at 40 weeks of age. Control mice (white circle), STZ-50 mice (dark-gray square), STZ-150 (light-gray square). E: Kidney weight/body weight at 40 weeks of age. All Data are mean ± SD. *$P < 0.05$. N = 6 per each group.

disease, analysis of histological and functional changes is easier. However, in STZ-diabetic mouse the development of hyperglycemia is not consistent. Only half develop severe diabetes in 3 weeks after high-dose STZ injection. Moreover, in low-dose STZ mice, the survive rate is very low. Therefore, in STZ mice, because much more variation of renal lesions is observed, it is difficult to evaluate the nephropathy correctly and a larger number of mice are required to examine the renal disease statistically. (2) ICER Tg mouse stably expresses major clinical and pathological features of human diabetic nephropathy. The process of diabetic renal changes in this model is similar to those in humans: At 8 weeks, GFR was already increased and glomerular hypertrophy was prominent (the earliest stage of human diabetic nephropathy). At 20 weeks, a peak in GFR and an increase in the urinary albumin excretion rate were seen (the early to middle stage of human diabetic nephropathy). At 40 weeks, messangial matrix expansion, diffuse glomerular sclerotic lesions and GBM thickening, declined GFR, increased urinary albumin excretion rate, lower serum albumin, and higher serum total cholesterol levels were observed (the advanced stage of human diabetic nephropathy) (Inada et al., 2005b). However, other characteristic diabetic lesion, such as nodular sclerotic lesions or exudative lesions seen in human diabetic nephropathy were not observed in this model. In contrast, STZ mice show mesangial expansion with time and glomerulosclerosis only in limited backgrounds (Breyer et al., 2005). (3) Mechanism of renal functional changes in ICER Tg mouse is different from those of STZ mice. Since ICER is expressed only in pancreatic β cells but not in other organs (Inada et al., 2004), it is feasible to investigate the specific effect of hyperglycemia in this model. However, in STZ-diabetic model the direct toxic effect of STZ cannot be excluded, as shown in the hepatic and renal changes. STZ is taken up by a glucose transporter into renal proximal tubular cells and generates nitric oxide (NO), which is likely to account for the non-specific cytotoxicity resulting in acute kidney tubular damage (Sadoff, 1970; Kwon et al., 1994; Tay et al., 2005). Thus, the renal damage on STZ-diabetic mice is due to complex separate toxic effects of STZ and hyperglycemia (Lee et al., 1974; Churchill et al., 1993). (4) The ICER model is easy to produce: they can easily be crossed with normal C57BL/6 mice, and identified by the blood glucose measurements. Once ICER Tg mice develop diabetes by 2–3 weeks of age, they can survive without insulin injections. Since it is hard for low-dose STZ-diabetic mice to survive with uncontrolled blood glucose for a long time, we are often obligated to control blood glucose levels by daily insulin injections and even with this optimal glucose control is difficult to achieve. In addition, insulin might have other effect upon the diabetic renal changes.

In summary, we demonstrated an advantage of our diabetic mouse model compared with STZ mice. ICER Tg mice thus provide an excellent experimental diabetes model for studying

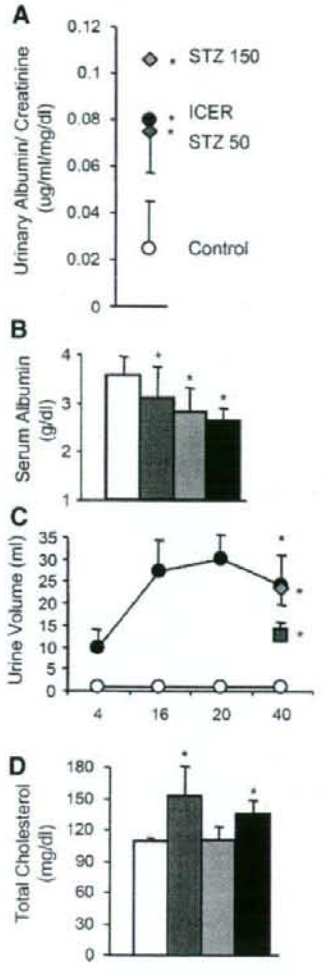

Fig. 8. Renal functional change in STZ-diabetic and ICER Tg mice. A: Urinary albumin excretion rate, (C) urine volume curve, and (D) total serum cholesterol was increased at 40 weeks of age. B: Serum albumin was low: from left, control (white), STZ-50 (dark-gray), STZ-150 (light-gray), ICER Tg mice (black). (C) STZ-150 (light-gray diamond), STZ-50 mice (dark-gray square). All Data are mean ± SD. *$P < 0.05$. N = 6 per each group.

the pathogenesis and to assessing the treatment of diabetic nephropathy and other complications, replacing STZ-induced diabetes animals.

Acknowledgments

We thank Hideo Uchiyama (Taigenkai Hospital) for technical assistance. This study was supported by Scientific Research (19890150) and Creative Scientific Research (NP10NPO201) from The Ministry of Education, Culture, Sports, Science and Technology (MEXT), "Research for the Future Program" from the Japan Society for the Promotion of Science (JSPS-RFTF97I00201), Japan Diabetes Foundation, and Mochida Memorial Foundation.

Literature Cited

Bonner-Weir S. 2000. Islet growth and development in the adult. J Mol Endocrinol 24:297–302.
Breyer MD, Bottinger E, Brosius FC III, Coffman TM, Harris RC, Heilig CW, Sharma K. 2005. AMDCC: Mouse models of diabetic nephropathy. J Am Soc Nephrol 16:27–45.
Breyer MD, Zhonghua Qi, Tchekneva E. 2006. Diabetic nephropathy: leveraging mouse genetics. Curr Opin Nephrol Hypertens 15:227–232.
Brondum E, Nilsson H, Aalkjaer C. 2005. Functional abnormalities in isolated arteries from Goto-Kakizaki and streptozotocin-treated diabetic rat models. Horm Metab Res 1:56–60.
Churchill P, Churchill M, Bidani A, Dunbar J, Jr. 1993. Streptozotocin-induced renal hemodynamic changes in isogenic Lewis rats: A kidney transplant study. Am J Physiol 264:F100–F105.
Doi T, Hattori M, Agodoa LY, Sato T, Yoshida H, Striker LJ, Striker GE. 1990. Glomerular lesions in nonobese diabetic mouse: Before and after the onset of hyperglycemia. Lab Invest 63:204–212.
Foulkes NS, Borrelli E, Sassone-Corsi P. 1991. CREM gene: Use of alternative DNA-binding domains generates multiple antagonists of cAMP-induced transcription. Cell 64:739–749.
Imaeda A, Kaneko T, Aoki T, Kondo Y, Nagase H. 2002. DNA damage and the effect of antioxidants in streptozotocin-treated mice. Food Chem Toxicol 40:979–987.
Inada A, Yamada Y, Someya Y, Kubota A, Yasuda K, Ihara Y, Kagimoto S, Kuroe A, Tsuda K, Seino Y. 1998. Transcriptional repressors are increased in pancreatic islets of type 2 diabetic rats. Biochem Biophys Res Commun 253:712–718.
Inada A, Someya Y, Yamada Y, Ihara Y, Kubota A, Ban N, Watanabe R, Tsuda K, Seino Y. 1999. The cyclic AMP response element modulator family regulates the insulin gene transcription by interacting with transcription factor IID. J Biol Chem 274:21095–21103.
Inada A, Hamamoto Y, Tsuura Y, Miyazaki J, Toyokuni S, Ihara Y, Nagai K, Yamada Y, Bonner-Weir S, Seino Y. 2004. Overexpression of inducible cyclic AMP early repressor inhibits transactivation of genes and cell proliferation in pancreatic β cells. Mol Cell Biol 24:2831–2841.
Inada A, Weir GC, Bonner-Weir S. 2005a. Induced ICER Iy down-regulates cyclin A expression and cell proliferation in insulin-producing β cells. Biochem Biophys Res Commun 329:925–929.
Inada A, Nagai K, Arai H, Miyazaki J, Nomura K, Kanamori H, Toyokuni S, Yamada Y, Bonner-Weir S, Weir GC, Fukatsu A, Seino Y. 2005b. Establishment of a diabetic mouse model with progressive diabetic nephropathy. Am J Pathol 167:327–336.
Iwase M, Nunoi K, Sadoshima S, Kikuchi M, Fujishima M. 1989. Liver, kidney and islet cell tumors in spontaneously hypertensive and normotensive rats treated neonatally with streptozotocin. Tohoku J Exp Med 159:83–90.
Janssen U, Riley SG, Vassiliadou A, Floege J, Phillips AO. 2003. Hypertension superimposed on type II diabetes in Goto-Kakizaki rats induces progressive nephropathy. Kidney Int 63:2162–2170.
Junod A, Lambert AE, Orci L, Pictet R, Gonet AE, Renold AE. 1967. Studies of the diabetogenic action of streptozotocin. Proc Soc Exp Biol Med 126:201–205.
Koulmanda M, Qipo A, Chebrolu S, O'Neil J, Auchincloss H, Smith RN. 2003. The effect of low versus high dose of streptozotocin in cynomolgus monkeys (Macaca fascilularis). Am J Transpl 3:267–272.
Kwon NS, Lee SH, Choi CS, Kho T, Lee HS. 1994. Nitric oxide generation from streptozotocin. FASEB J 8:529–533.
Lee CS, Mauer SM, Brown DM, Sutherland DE, Michael AF, Najarian JS. 1974. Renal transplantation in diabetes mellitus in rats. J Exp Med 139:793–800.
Lee HB, Seo JY, Yu MR, Uh ST, Ha H. 2007. Radical approach to diabetic nephropathy. Kidney Int 106:S67–S70.
Like AA, Rossini AA. 1976. Streptozotocin-induced pancreatic insulitis: New model of diabetes mellitus. Science 193:415–417.
Like AA, Appel MC, Williams RM, Rossini AA. 1978. Streptozotocin-induced pancreatic insulitis in mice. Morphologic and physiologic studies. Lab Invest 38:470–486.
Nagai K, Arai H, Yanagita M, Matsubara T, Kanamori H, Nakano T, Iehara N, Fukatsu A, Kita T, Doi T. 2003. Growth arrest-specific gene 6 is involved in glomerular hypertrophy in the early stage of diabetic nephropathy. J Biol Chem 278:18229–18234.
Nagasao J, Yoshioka K, Amasaki H, Tsujio M, Ogawa M, Taniguchi K, Mutoh K. 2005. Morphological changes in the rat endocrine pancreas within 12 h of intravenous streptozotocin administration. Anat Histol Embryol 34:42–47.
Nukatsuka M, Yoshimura Y, Nishida M, Kawada J. 1990. Importance of the concentration of ATP in rat pancreatic beta cells in the mechanism of streptozotocin-induced cytotoxicity. J Endocrinol 127:161–165.
Palm F. 2006. Intratenal oxygen in diabetes and a possible link to diabetic nephropathy. Clin Exp Pharm Phys 33:997–1001.
Palm F, Ortsater H, Hansell P, Liss P, Carlsson PO. 2004. Differentiating between effects of streptozotocin per se and subsequent hyperglycemia on renal function and metabolism in the streptozotocin-diabetic rat model. Diabetes Metab Res Rev 20:452–459.
Sadoff L. 1970. Nephrotoxicity of streptozotocin (NSC-85998). Cancer Chemother Rep 54:457–459.
Schein P, Kahn R, Gorden P, Wells S, Devita VT. 1973. Streptozotocin for malignant insulinomas and carcinoid tumor. Report of eight cases and review of the literature. Arch Intern Med 132:555–561.
Sotnikova R, Nosalova V, Stefek M, Stolc S, Gajdosik A, Gajdosikova A. 1999. Streptozotocin diabetes-induced changes in aorta, peripheral nerves and stomach of Wistar rats. Gen Physiol Biophys 18:155–162.
Szkudelski T. 2001. The mechanism of alloxan and streptozotocin action in B cells of the rat pancreas. Physiol Res 50:536–546.
Tay YC, Wang Y, Kairaitis L, Rangan GK, Zhang C, Harris DC. 2005. Canmurine diabetic nephropathy be separated from superimposed acute renal failure? Kindney Int 68:391–398.
Tesch GH, Nikolic-Paterson DJ. 2006. Recent insights into experimental mouse models of diabetic nephropathy. Nephron Exp Nphrol 104:e57–e62.
Tochino Y. 1987. The NOD mouse as a model of type I diabetes. Crit Rev Immunol 8:49–81.
Tojo A, Asaba K, Onozato ML. 2007. Suppressing renal NADPH oxidase to trear diabetic nephropathy. Expert Opin Ther targets 11:1011–1018.
Tomohiro T, Kumai T, Sato T, Takeba Y, Kobayashi S, Kimura K. 2007. Hypertension aggravates glomerular dysfunction with oxidative stress in a rat model of diabetic nephropathy. Life Sci 80:1364–1372.

Velasquez MT, Kimmel PL, Michaelis OE IV. 1990. Animal models of spontaneous diabetic kidney disease. FASEB J 4:2850–2859.
Wang T, Fontenot RD, Soni MG, Bucci TJ, Mehendale HM. 2000. Enhanced hepatotoxicity and toxic outcome of thioacetamide in streptozotocin-induced diabetic rats. Toxicol Appl Pharmacol 166:92–100.
Williamson JR, Chang K, Tilton RG, Prater C, Jeffrey JR, Weigel C, Sherman WR, Eades DM, Kilo C. 1987. Increased vascular permeability in spontaneously diabetic BB/W rats and in rats with mild versus severe streptozocin-induced diabetes. Prevention by aldose reductase inhibitors and castration. Diabetes 36:813–821.
Yokozawa T, Nakagawa T, Wakaki K, Koizumi F. 2001. Animal model of diabetic nephropathy. Exp Toxicol Pathol 53:359–363.
Zatz R, Meyer TW, Rennke HG, Brenner BM. 1985. Predominance of hemodynamic rather than metabolic factors in the pathogenesis of diabetic glomerulopathy. Proc Natl Acad Sci USA 82:5963–5967.

Acute Renal Failure After Exercise in a Japanese Sumo Wrestler With Renal Hypouricemia

AKIRA MIMA, MD, PHD; KIMIYOSHI ICHIDA, MD, PHD; TAKESHI MATSUBARA, MD, PHD; HIROSHI KANAMORI, MD; EMI INUI, MD; MISA TANAKA, MD, PHD; YUMI MANABE, MD; NORIYUKI IEHARA, MD, PHD; YOSHINORI TANAKA, MD; MOTOKO YANAGITA, MD, PHD; ATSUKO YOSHIOKA, MD; HIDENORI ARAI, MD, PHD; MASASHI KAWAMURA, MD; KATSUMASA USAMI, MD; TATSUO HOSOYA, MD, PHD; TORU KITA, MD, PHD; ATSUSHI FUKATSU, MD, PHD

ABSTRACT: Familial renal hypouricemia is a hereditary disease characterized by extraordinary high renal uric acid clearance and is associated with acute renal failure (ARF). An 18-year-old sumo wrestler developed ARF after anaerobic exercise. Several hours after the exercise, he had a pain in the loins with oliguria, headache, and nausea. On admission, his serum uric acid was decreased despite the elevation of serum creatinine (9.5 mg/dL). The level of creatine kinase was normal and there was no myoglobinuria or urolithiasis. Magnetic resonance imaging showed no significant abnormality. Renal function improved completely within 2 weeks of hydration treatment. After remission, hypouricemia became obvious (1.0 mg/dL) from the initial level of uric acid (6.1 mg/dL) and fractional excretion of uric acid was 49%. Polymerase chain reaction of a urate anion exchanger known to regulate blood urate level (*SLC22A12* gene: *URAT1*) demonstrated that homozygous mutations in exon 4 (W258X). Both parents showed heterozygous mutation of the *URAT1* gene, but both siblings showed no mutation. Thus, we describe a Japanese sumo wrestler of familial renal hypouricemia complicated with anaerobic exercise-induced ARF, with definite demonstration of genetic abnormality in the responsible gene, *URAT1*. **KEY INDEXING TERMS:** Renal hypouricemia; Acute renal failure; *URAT1* gene. **[Am J Med Sci 2008; 336(6):512–514.]**

Hypouricemia, defined as low levels of serum urate (less than 2.0 mg/dL), has been recognized as a predisposition toward exercise-induced acute renal failure (ARF). The incidence of hypouricemia is reported to be 0.16% in men and 0.23% in women among normal adults,[1] and to be 2.54% in hospitalized patients.[2] Exercise-induced ARF has been increasing, although hypouricemia is not a rare condition. Patients complain of severe loin pain with nausea and vomiting after anaerobic exercise.[3] Although some patients need to have dialysis because of ARF, short-term prognosis of these patients seems to be good.[4–7] Recently, patients with idiopathic renal hypouricemia are found to have mutations in the gene (*SLC22A12*) encoding for human urate transporter 1 (hURAT1), and several *URAT1* genetic mutations have been revealed in patients with hypouricemia.[8,9]

In this article, we report a Japanese sumo wrestler with anaerobic exercise-induced ARF associated with renal hypouricemia caused by a mutation in the *URAT1* gene.

Case Report

The patient is an 18-year-old Japanese sumo wrestler and his patients are healthy. He was born after normal pregnancy and delivery. He had no family history of ARF or any renal diseases. He was admitted to a hospital because of nausea, vomiting, headache, and severe loin pain after anaerobic exercise. On admission, serum BUN and creatinine were elevated to 74 mg/dL and 9.5 mg/dL, respectively, with a slight decrease in serum uric acid (6.1 mg/dL). The level of creatine kinase was normal and there was no myoglobinuria or urolithiasis. The urine output was 200 to 300 mL/day. After hydration therapy, he was transferred to our hospital for further examination. On admission to our hospital, his height and weight were 165 cm and 100 kg, respectively. He had no oliguria in our hospital. Physical examination revealed no abnormalities. Laboratory test of this patient showed a hemoglobin 15.0 g/dL, hematocrit 44.8%, leukocyte count 7100/μL with normal differentiation, platelet 217,000/μL, total protein 7.2 g /dL, serum sodium 143

From the Department of Nephrology (AM, TM, HK, EI, MT, YM, NI, YT, MY, AY, AF), Kyoto University Graduate School of Medicine, Kyoto, Japan; Division of Kidney and Hypertension, Department of Internal Medicine (KI, TH), Jikei University School of Medicine, Tokyo, Japan; Departments of Geriatric Medicine (HA) and Cardiovascular Medicine (TK), Kyoto University Graduate School of Medicine, Kyoto, Japan; Department of Internal Medicine (MK), Kochi Prefectural Hata Kenmin Hospital, Kochi, Japan; and Department of Internal Medicine (KU), Ijinkai Takeda General Hospital, Kyoto, Japan.

Submitted October 21, 2007; accepted in revised form November 28, 2007.

Correspondence: Akira Mima, M.D., Ph.D., Departments of Nephrology, Kyoto University Graduate School of Medicine, 54 Kawahara-cho, Shogoin, Sakyo-ku, Kyoto 606-8507, Japan (E-mail: amima@kuhp.kyoto-u.ac.jp).

Table 1. Laboratory Data of Family Members

	Serum Uric Acid (S-UA) (mg/dL)	Urine Uric Acid (U-UA) (mg/dL)	Creatinine Clearance (Ccr) (mL/min)	FEUA (%)
Present case	1.0	44	116.4	52
Father	4.7	61.2	118.5	15.2
Mother	3.2	21.1	129.9	5.7
Sister	4.7	78	111.4	8.1
Paternal grandfather	4.7	20.5	53.5	5.8
Maternal grandfather	3.5	26	122.1	6.5

mEq/L, serum potassium 4.0 mEq/L, serum chloride 106 mEq/L, serum calcium 9.4 mg/dL, serum phosphate 3.9 mg/dL, serum BUN 12 mg/dL, serum creatinine 1.3 mg/dL, serum uric acid 1.0 mg/dL, bicarbonate 24.6 mmol/L, serum creatinine kinase 83 U/L, antistreptolysin O 232 IU/mL, and fractional excretion of sodium 0.59%. The following parameters were within normal limits or negative: total cholesterol, aspirate aminotransferase, alanine aminotransferase, lactate dehydrogenase, C-reactive protein, antinuclear antibody, serum hemolytic complement activity, hepatitis B surface antigen, hepatitis C antibody. On urinalysis glucosuria, aminoaciduria or crystallization was not found, and there were no other abnormal data observed, except significantly higher fractional excretion of uric acid (FEUA) (52%; normal 7%–12%). These results suggested that diagnosis of renal hypouricemia, not existing dysfunction of the proximal renal tubule leading excessive urinary losses of amino acids, glucose, bicarbonate, phosphate, and uric acid. Test with the pyrazinamide or probenecid, which are inhibitors of the renal urate transporting systems were not performed.

Electrocardiogram and X-ray films of chest and abdomen were normal. An abdominal magnetic resonance imaging scan did not reveal slight swollen kidney, but wedge-shaped images were not recognized.

Table 1 shows the laboratory examination data of the patient and his family members. The levels of serum uric acid and FEUA were within normal limits in his grandfathers, parents, and sister. The mutational analysis of the *SLC22A12* gene was performed after obtaining informed consent and revealed that he was homozygous for W258X. His grandfathers and parents were heterozygous for W258X, although his sister was wild type (Figures 1 and 2). We guided him to warm up before exercise. Although marked hypouricemia (0.8–1.0 mg/dL) has persisted, a similar ARF episode has not occurred.

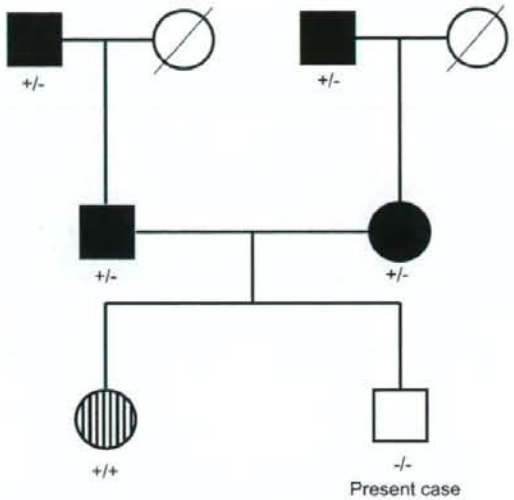

Figure 1. Mutations of *SLC22A12* (*URAT1*). Men are denoted by squares, women by circles. Clinical status is indicated as follows: typical clinical manifestations of hereditary renal hypouricemia (homozygous): thick open squares; heterozygous mutation: solid symbols; unaffected individual: hatched symbol.

Discussion

Hypouricemia is defined as serum uric acid concentrations lower or equal to 2 mg/dL.[10] It is a fairly common abnormality, which occurs in 0.5%–4.0% of general populations and occurs in about 1% of hospitalized patients .[2,11,12] It can be caused by reduced uric acid production or by reduced renal tubular reabsorption of filtered uric acid. The incidence of renal hypouricemia has been reported to fall in the range 0.12% to 0.72%.[13]

Renal hypouricemia is a hereditary condition of increased renal urate clearance caused by an isolated inborn error of membrane transport for urate in the renal proximal tubule. Recently, Enomoto et al[8] proposed a model of indirect coupling of sodium and urate transport and identified in the human kidney, URAT1, encoded by *SLC22A12*. Intracellular accumulation of sodium and urate for which URAT1 has affinity will favor the reabsorption of urate in exchange for anions, which move down their electromechanical gradients into the tubular lumen. Most patients with idiopathic renal hypouricemia have loss-of-function mutations in *SLC22A12*.[9] In this study, the parents of patient, who are heterozygous for W258X, had normal FEUA without hypouricemia. In contrast, the patient, a homozygous for W258X had much more severe hypouricemia with much higher FEUA than them.

Most mutations in *SLC22A12* have been detected in hypouricemic patients and the W258X mutation, which produces a nonfunctioning truncated protein that lacks half of the mature protein, is the predominant *SLC22A12* mutation,[8] and was detected in 40 of 54 mutated alleles. About half of those with *SLC22A12* mutations were homozygotes, about 30% were compound heterozygotes, and the rest were heterozygotes[8,9] As in this case, the serum uric acid level was lower than 1.0 mg/dL in almost all homozygotes and compound heterozygoutes.

Exercise-induced ARF with renal hypouricemia has typical clinical features; ARF can develop after acute anaerobic exercise in conjunction with severe loin pain, but without evidence of massive rhabdomyolysis.[4–7] Precise mechanisms of this nephropathy are still unknown, but one possibility is that an increase of oxygen free radicals produced during exercise leads to renal tissue

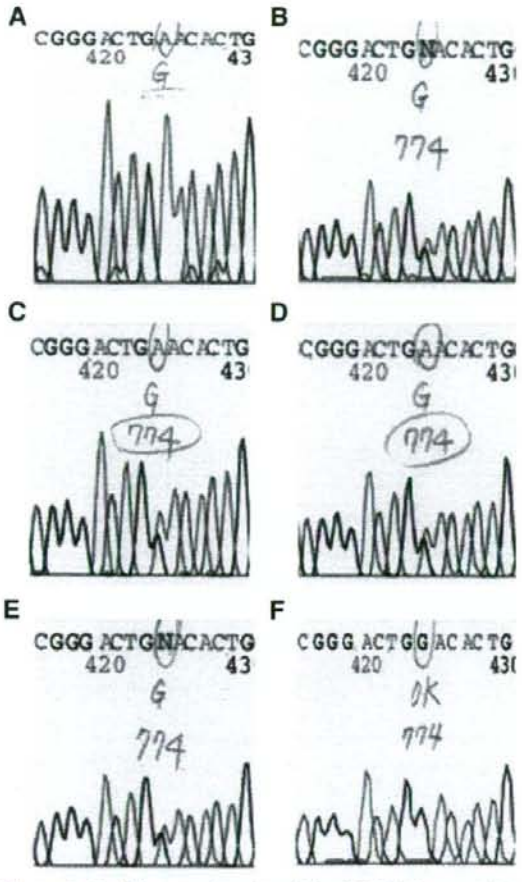

Figure 2. Partial sequencing data of the *SLC22A12* gene. (A) A homozygous G to A transition at nucleotide 774 in exon 4, which results in a codon change of W258X, in present case. (B) A heterozygous transition at nucleotide 774 (W258X) in patient's father. (C) A heterozygous G to A transition at nucleotide 774 (W258X) in patient's mother. (D) A heterozygous G to A transition at nucleotide 774 (W258X) in patient's paternal grandfather. (E) A heterozygous transition at nucleotide 774 (W258X) in patient's maternal grandfather. (F) A normal sequence in patient's sister.

damage.[14] Because uric acid seems to be a strong antioxidant and a scavenger of free radicals, that could spoil the renal function during anaerobic exercise.[14] Our sequence analysis of the *URAT1* gene of all family members showed that the patient had homozygous mutations in exon 4 (W258Stop), resulting in premature truncated URAT1 protein, whereas his grand fathers and parents showed heterozygous mutations. These phenomena led that healthy grand fathers and parents with the heterozygous *SLC22A12* mutation whose serum urate level and FEUA were in the normal range.

Although it is not known whether mutations in the *URAT1* gene can explain several types of a urate-transporting defect in renal hypouricemic patients such as so called four-component model (presecretory reabsorption defect, postsecretpry reabsorption defect, or hyper secretion defect). Moreover, patients with presecretory reabsorption defect do not always show exercise-induced ARF. Differences in mutations of the *URAT1* gene might be responsible for the difference in the clinical features. Further investigations will be needed to detect new mutations or to detect unknown urate transporter. Interestingly, Ichida et al have shown 8 new *SLC22A12* renal hypouricemia mutations.

In summary, we report a Japanese sumo wrestler who often takes anaerobic exercise-induced ARF associated with renal hypouricemia. Furthermore, it is recognized that he has a homozygous mutation of *SLC22A12*.

Acknowledgments

We thank Takako Pezzotti, Maki Watanabe, and Ayumi Hosotani (Kyoto University) for excellent technical assistance.

References

1. **Erley CM, Hirschberg RR, Hoefer W, et al.** Acute renal failure due to uric acid nephropathy in a patient with renal hypouricemia. Klin Wochenschr 1989;67:308–12.
2. **Ogino K, Hisatome I, Saitoh M, et al.** Clinical significance of hypouricemia in hospitalized patients. J Med 1991;22:76–82.
3. **Ohta T, Sakano T, Ogawa T, et al.** Exercise-induced acute renal failure with renal hypouricemia: a case report and a review of the literature. Clin Nephrol 2002;58:313–6.
4. **Ishikawa I.** Acute renal failure with severe loin pain and patchy renal ischemia after anaerobic exercise in patients with or without renal hypouricemia. Nephron 2002;91:559–70.
5. **Ishikawa I, Sakurai Y, Masuzaki S, et al.** Exercise-induced acute renal failure in 3 patients with renal hypouricemia. Nippon Jinzo Gakkai Shi 1990;32:923–8.
6. **Igarashi T, Sekine T, Sugimura H, et al.** Acute renal failure after exercise in a child with renal hypouricaemia. Pediatr Nephrol 1993;7:292–3.
7. **Hisanaga S, Kawamura M, Uchida T, et al.** Exercise-induced renal failure in a patient with hyperuricosuric hypouricemia. Nephron 1994;66:475–6.
8. **Enomoto A, Wempe MF, Tsuchida H, et al.** Molecular identification of a novel carnitine transporter specific to human testis. Insights into the mechanism of carnitine recognition. J Biol Chem 2002;277:36262–71.
9. **Ichida K, Hosoyamada M, Hisatome I, et al.** Clinical and molecular analysis of patients with renal hypouricemia in Japan-influence of URAT1 gene on urinary urate excretion. J Am Soc Nephrol 2004;15:164–73.
10. **Sperling O.** Renal hypouricemia: classification, tubular defect and clinical consequences. Contrib Nephrol 1992;100:1–14.
11. **Maesaka JK, Fishbane S.** Regulation of renal urate excretion: a critical review. Am J Kidney Dis 1998;32:917–33.
12. **Bairaktari ET, Kakafika AI, Pritsivelis N, et al.** Hypouricemia in individuals admitted to an inpatient hospital-based facility. Am J Kidney Dis 2003;41:1225–32.
13. **Hisatome I, Ogino K, Kotake H, et al.** Cause of persistent hypouricemia in outpatients. Nephron 1989;51:13–16.
14. **Ames BN, Cathcart R, Schwiers E, et al.** Uric acid provides an antioxidant defense in humans against oxidant- and radical-caused aging and cancer: a hypothesis. Proc Natl Acad Sci USA 1981;78:6858–62.

A comparative study of the diagnostic accuracy of ELISA systems for the detection of anti-neutrophil cytoplasm antibodies available in Japan and Europe

T. Ito-Ihara[1,2,3], E. Muso[1], S. Kobayashi[4], K. Uno[2], N. Tamura[5], Y. Yamanishi[6], A. Fukatsu[7], R.A. Watts[8], D.G.I. Scott[9], D.R.W. Jayne[10], K. Suzuki[11], H. Hashimoto[5]

[1]Department of Nephrology and Dialysis, Kitano Hospital, Tazuke Kofukai Medical Research Institute, Osaka, Japan; [2]Louis Pasteur Centre for Medical Research, Kyoto, Japan; [3]Musculoskeletal Research Group, School of Clinical Medical Sciences, Newcastle University, Newcastle upon Tyne, UK; [4]Department of Rheumatology, Juntendo Koshigaya Hospital, Saitama, Japan; [5]Department of Internal Medicine and Rheumatology, Juntendo University, School of Medicine, Tokyo, Japan; [6]Department of Rheumatology, Hiroshima City Hospital, Hiroshima, Japan; [7]Department of Nephrology, Kyoto University Graduate School of Medicine, Kyoto, Japan; [8]Department of Rheumatology, Ipswich Hospital, Suffolk, UK; [9]Department of Rheumatology, Norfolk and Norwich University Hospital, Norfolk, UK; [10]Lupus and Vasculitis Clinic, Addenbrookes' Hospital, Cambridge, UK; [11]National Institute of Infectious Diseases (NIID-NIH), Tokyo, Japan and Chiba University Graduate School of Medicine, Inflammation Program, Department of Immunology, Chiba, Japan.

Abstract

Objectives

Primary systemic vasculitis associated with anti-neutrophil cytoplasm antibodies (ANCA) differs in its frequency and clinical expression between Japan and Europe. We sought to ascertain whether such differences arise from the performance of enzyme-linked immunosorbent assays (ELISAs) for ANCA.

Methods

Plasma samples from 64 consecutive Japanese patients with a clinical and histological diagnosis of primary systemic vasculitis including microscopic polyangiitis (MPA; n=52), Churg-Strauss syndrome (CSS; n=1), and Wegener's granulomatosis (WG; n=11), or those from disease controls with non-vasculitic glomerulonephritis (n=54) and healthy controls (n=55) were tested for the presence of myeloperoxidase (MPO) by ELISAs available in Japan (Nipro and MBL) and compared with those in Europe (Wieslab). The sensitivity and specificity were calculated for each ELISA, and its diagnostic performance was assessed by receiver operating characteristic curve analysis.

Results

The sensitivity and specificity of either MPO-ANCA assays for a diagnosis of MPA were 90.4% and 98.2% (Nipro), 88.2% and 96.3% (MBL), and 86.5% and 99.1% (Wieslab). The overall diagnostic performance, assessed as the area under curve of the MPO-ANCA ELISAs for MPA were 0.946±0.022 (Nipro), 0.970±0.017 (MBL), and 0.971±0.017 (Wieslab), while that of PR3-ANCA ELISAs for WG were 0.986±0.025 (Nipro), 0.993±0.017 (MBL), and 0.916±0.059 (Wieslab).

Conclusions

The MPO-ANCA ELISAs commercially available in Japan exhibited high sensitivity and specificity for the diagnosis of ANCA-associated vasculitides and provided similar diagnostic value to those in Europe. These results facilitate further international comparison of ANCA-associated vasculitides between Japanese and European populations.

Key words

MPO-ANCA, PR3-ANCA, Capture ELISA, streptavidin-coated ELISA, ANCA-associated vasculitides (AAV), systemic vasculitis.

Clinical and Experimental Rheumatology 2008; **26**: 1027-1033.

Toshiko Ito-Ihara MD, PhD
Eri Muso MD, PhD
Shigeto Kobayashi MD, PhD
Kazuko Uno PhD
Naoto Tamura MD, PhD
Yuji Yamanishi MD, PhD
Atsushi Fukatsu MD, PhD
Richard A. Watts DM
David G.I. Scott MD, FRCP
David R.W. Jayne MD, FRCP
Kazuo Suzuki PhD
Hiroshi Hashimoto MD, PhD

This study was supported by grant no. SH44410, the Japan Health Sciences Foundation with a grant for "Research on Health Sciences focusing on Drug Innovation, International Collaborative Research", the Ministry of Health, Labour and Welfare in Japan from 2004 to 2006; a grant for "Research on Regulatory Science of Pharmaceuticals and Medical Devices", the Ministry of Health, Labour and Welfare in Japan; the "Dispatch program Abroad for Japanese Researchers 2006" from the Society of Japanese Pharmacopoeia; a research grant from Japan Society for Promotion Science and Ministry of Education, Culture, Sports, Science and Technology, Grant in Aid for Young Scientists (B) no. 18790584 (to T.I.); the British Council Japan Association Fellowship 2007 (to T.I.); and the Daiwa Foundation Small Grant from The Daiwa Anglo-Japanese Foundation (to T.I., D.J., E.M.).

Please address reprint requests and correspondence to:
Professor Eri Muso,
The Tazuke Kofukai Medical Research Institute, Kitano Hospital,
2-4-20 Ogimachi, Kitaku, Osaka, 530-8480, Japan.
E-mail: muso@kitano-hp.or.jp

Received on October 15, 2007; accepted in revised form on May 30, 2008.

© Copyright CLINICAL AND EXPERIMENTAL RHEUMATOLOGY 2008.

Competing interests: none declared.

Introduction

Anti-neutrophil cytotoplasm antibodies (ANCA) are found in a high percentage of patients with Wegener's granulomatosis (WG), microscopic polyangiitis (MPA) and Churg-Strauss syndrome (CSS) and are used as diagnostic markers for these diseases, which are also termed the ANCA-associated vasculitides (AAV). On the indirect immunofluorescence (IIF) test, ANCA usually exhibits either a granular cytoplasmic pattern (C-ANCA) or a peri-nuclear pattern (P-ANCA). C-ANCA positivity is characteristically observed in patients with WG mostly directed against proteinase 3 (PR3-ANCA), while the P-ANCA that frequently occur in MPA are in general directed against myeloperoxidase (MPO-ANCA). ANCA detected by IIF are also apparent in several other inflammatory conditions; in these cases, ANCA as detected by IIF is not specific for vasculitis. Therefore, ANCA should be demonstrated by using a combination of IIF and ELISA (1, 2).

The major problem with the current application of ANCA ELISA systems is the lack of international standard sera and the lack of international standardization of assay systems. Unfortunately, commercially available ELISA systems have a wide range of performance characteristics and employ arbitrary units determined by each manufacturer (3). When interpreting an ANCA test, therefore, the clinician must take into account the differences between the ELISA systems.

In Japan, three kinds of MPO-ANCA and PR3-ANCA ELISA systems are currently available as extracorporeal diagnostic agents authorized by the Ministry of Health and Welfare of Japan. Comparison of these ELISA systems with those commonly used in Europe is essential for international collaboration and for epidemiological and clinical research.

In the present study we compared the sensitivity and specificity of two major commercially available ANCA ELISA systems in Japan and one of the most widely used systems in Europe for MPO-ANCA and PR3-ANCA using plasma obtained from Japanese patients with a clinical and histological diagnosis of WG, MPA, or CSS. We also assessed the correlation of ANCA values among ELISA systems. This study aims to further validate the role of ANCA assays available in Japan and permit comparative international studies involving Japanese patients with AAV.

Patients and methods

Patient population and diagnostic criteria

The plasma samples were derived from newly diagnosed patients with primary systemic vasculitis (PSV) including WG, MPA, or CSS in accordance with the American College of Rheumatology (ACR) classification criteria and Chapel Hill consensus criteria (CHCC) with reference of EMEA algorithm method (4-7). We modified the algorithm to be irrespective of positivity of ANCA for the purpose of this study. 64 consecutive patients who had newly diagnosed disease were enrolled (MPA, n=52; CSS, n=1; WG, n=11) in the Department of Nephrology and Cardiovascular Medicine at Kyoto University hospital (Kyoto, Japan) between June 1999 and June 2000, in the Department of Nephrology and Dialysis and in the Department of Clinical Immunology and Rheumatology in Tazuke Kofukai Medical Research Institute Kitano Hospital (Osaka, Japan) between July 2000 and Apr 2008, and in the Department of Internal Medicine and Rheumatology in Juntendo University Hospital (Tokyo, Japan) between January 2005 and January 2006. The same number of plasma samples (n=58) were obtained during the untreated phase when the patients showed an acute exacerbation of symptom of organ involvement consistent with active vasculitis before the start of any immunosuppressive treatment. All patients had active disease at enrollment defined as Birmingham Vasculitis Activity Score (BVAS) of at least 4 (8). Plasma samples were also obtained from these patients in the follow up period between one week and six months after the start of immunosuppressive treatment (MPA, n=80; WG, n=2). All the patients were systematically assessed for potential subclinical granulomatous disease with diagnostic

imaging as well as ENT consultation. Confirmatory organ histological biopsies were available in eight out of 11 patients with WG including four renal biopsies, two lung biopsies, and two biopsies from nodules of paranasal sinuses. Renal biopsies were performed in all the MPA and CSS patients and revealed that all of them showed renal involvement.

For disease controls, we also assayed plasma from 64 consecutive new patients with non-vasculitic glomerulonephritis who had a renal biopsy in Kitano Hospital in this study period; diagnoses included IgA nephropathy (n=18), non-IgA type mesangioproliferative glomerulonephritis (n=5), endocapillary glomerulonephritis (n=1), interstitial nephritis (n=2), hepatitis C virus-related nephritis (n=1), membranoproliferative glomerulonephritis (n=3), membranous nephropathy (n=4), focal glomerulosclerosis (n=2), minimal change nephrotic syndrome (n=3), diabetic nephropathy (n=2), amyloidosis (n=1), malignant hypertension (n=1), nephrosclerosis (n=3), pseudo-Bartter syndrome (n=1), antiphospholipid syndrome (n=1), and lupus nephritis (n=6). None of the disease control patients were receiving immunosuppressive therapy at the time of sampling.

As healthy controls, the plasma samples from 55 people who received regular physical checkup in the clinic of Louis Pasteur Centre for Medical Research and had not have any diseases until 2004 were enrolled in this study.

This study was carried out in accordance with the 1975 Declaration of Helsinki of the World Medical Association. The design of the work has been approved by the ethical committee of the hospitals and clinic involved and each patient gave written informed consent for participation in the study. All plasma samples were fully spun down to remove fibrin clots preventing non-specific reaction and were stored at -80°C until tested.

Methods of ANCA detection

All assays for MPO-, PR3-ANCA, and IIF were performed according to the manufacturers' instructions.

Nipro MPO- and PR3-ANCA ELISA. Nipro Nephroscholar MPO-ANC II kit (Nipro, Osaka, Japan; authorization number of diagnostic drugs and medications in Japan No. 212000AMZ00598000) has been developed in Japan. Briefly, The 1:500 diluted samples and biotinylated MPO antigen solution (0.1 mg/well) were applied onto the plate coated with Streptavidine and incubated for 1 hour at room temperature. The binding of MPO-ANCA to MPO antigens purified from human sputum was assessed using alkaline phosphatase (AP)-labeled polyclonal goat anti-human IgG with p-Nitrophenyl phosphate disodium in diethanolamine as a substrate. After adding sodium hydrate as stop solution, the absorbance was measured photometrically at 405 nm. The cut-off value was 20 ELISA Unit/ml.

Nipro Nephroscholar PR3-ANC kit (authorization No. 21000AMY00275000) is imported from Euro-Diagnostica (Arnhem, The Netherlands and Malmö, Sweden) and the kit is equivalent to Immunoscan PR3-ANCA (Euro-Diagnostica). Purified PR3 from human neutrophils were directly coated onto a 96-well microplate. The 1:50 diluted samples were applied onto the plate coated with purified PR3. AP-labeled polyclonal pig anti-human IgG was added followed by p-Nitrophenyl phosphate disodium in diethanolamine as a substrate. The absorbance was measured photometrically at 405 nm. The cut-off value was 10 ELISA Unit/ml.

MBL MPO- and PR3-ANCA ELISA. MBL (Nagoya, Japan) has imported the kits from Binding Site (Birmingham, UK). MBL MPO-ANCA test (BS) Code No.BS-031 (Nagoya, Japan; authorization No. 21100AMY00184000) is equivalent to BINDAZYME™ Human Anti-MPO Enzyme Immunoassay kit, Code No.MK031 (Binding Site). MBL PR3-ANCA test (BS) Code No.BS-032 (authorization No. 21000AMY00075000) is equivalent to BINDAZYME™ Human Anti-PR3 Enzyme Immunoassay kit, Code No.MK032 (Binding Site). Each sample, diluted 1:101 in diluent was used. The binding of MPO- and PR3-ANCA to human purified antigens coated on the plate was assessed using anti-human IgG peroxidase conjugate and 3, 3', 5, 5'-tetramethylbenzidine (TMB) as a chromogen. The absorbance was measured photometrically at 450 nm and the cut-off values for MPO- and PR3-ANCA were 9.0 U/ml and 3.5 U/ml, respectively.

Wieslab MPO-ANCA and Capture PR3-ANCA ELISA. These kits were not permitted for diagnostic purpose in Japan as of Apr 2008. For detection of MPO-ANCA by direct ELISA, Wielisa MPO-ANCA MPO 103 (Wieslab AB, Lund, Sweden) was used. MPO purified from human neutrophils was coated on 96-well plates. Samples were diluted at 1:80 and antibody binding was assessed with AP-conjugated anti-human IgG. Values >25 units were considered to be positive.

Capture PR3-ANCA testing was performed with Wielisa capture PR3-ANCA, Cap-PR3 108X. Each sample, diluted 1:80 in PBS was used. The antigen-antibody complex was detected by AP-labeled anti-human IgG antibodies using p-nitrophenylphosphate as a chromogen with spectrophotometric reading at 405 nm. For this method,the cut-off value was 25 U/ml.

Indirect immunofluorescence (IIF) assay. ANCA detection by IIF was performed on commercially available slides of ethanol-fixed and formalin-fixed purified normal granulocytes. The MBL Fluoro ANCA test Code No.4710 and 4720 (MBL) are equivalent to the Binding Site ANCA ethanol kit Code FK016 and ANCA formalin kit Code FK017 (Binding Site), respectively. If peri-nuclear or nuclear immunofluorescence was detected on ethanol-fixed granulocyte, the IIF was repeated using formalin-fixed neutrophil preparations. Samples were interpreted as P-ANCA positive if they displayed cytoplasmic staining on formalin-fixed slides. Plasma sample of untreated PSV patients (n=64), disease controls (n=54), and healthy controls (n=55) were tested for positivity of IIF-ANCA.

Statistics

Performance characteristics were compared by receiver operating characteristic (ROC) curve analysis according to the method described by Hanley (9).

Table I. Sensitivity and Specificity of MPO-ANCA for MPA using clinical cut off value of each ELISA systems.

ELISA kit		Sensitivity	Specificity	AUC	AUC	*P* versus		
	Cut off	(% [95%CI])	(% [95%CI])	(± SE)	95% CI	Nipro	MBL	Wieslab
Nipro MPO-ANCA	20 U/ml	90.4 [79.0 - 96.8]	98.2 [93.5 - 99.7]	0.946 ± 0.022	0.899 - 0.976		0.282	0.269
MBL MPO-ANCA	9 U/ml	88.2 [76.1 - 95.5]	96.3 [90.9 - 99.0]	0.970 ± 0.017	0.930 - 0.990	0.282		0.951
Wieslab MPO-ANCA	25 U/ml	86.5 [74.2 - 94.4]	99.1 [95.0 - 99.8]	0.971 ± 0.017	0.932 - 0.991	0.269	0.951	

MPA: microscopic polyangiitis; ROC: receiver operating characteristics curve analysis; AUC: area under the ROC curve; SE: standard error; 95% CI: 95% confidence interval.
Sample size: MPA, n=52; disease controls, n=54; and healthy controls n=55.

Table II. Sensitivity and Specificity of PR3-ANCA for WG using clinical cut off value of each ELISA systems.

ELISA kit		Sensitivity	Specificity	AUC	AUC	*P* versus		
	Cut off	(% [95%CI])	(% [95%CI])	(± SE)	95% CI	Nipro	MBL	Wieslab
Nipro PR3-ANCA	10 U/ml	100.0 [71.3 - 100.0]	98.2 [93.5 - 99.7]	0.986 ± 0.025	0.945- 0.998		0.729	0.211
MBL PR3-ANCA	3.5 U/ml	100.0 [71.3 - 100.0]	95.4 [88.4 – 97.9]	0.993 ± 0.017	0.957 - 0.998	0.729		0.163
Wieslab PR3 ANCA	25 U/ml	90.9 [58.7 – 98.5]	99.1 [95.0 – 99.8]	0.916 ± 0.059	0.851 - 0.959	0.211	0.163	

WG: Wegener's granulomatosis; ROC: receiver operating characteristics curve analysis; AUC: area under the ROC curve; SE, standard error; 95% CI: 95% confidence interval.
Sample size: WG, n=11; disease controls, n=54; and healthy controls, n=55.

A difference of $p<0.05$ was considered to be statistically significant. The Software MedCalc® version 9.3.0.0. (MedCalc®, Mariakerke, Belgium) was used for statistical analysis. A correlation coefficient between MPO-ANCA ELISA kits was obtained using Statview-J software version 5.0 for Windows (SAS Institute Inc., Cary, NC). A probability value <0.05 was considered significant.

Results

Clinical diagnostic performance of MPO-ANCA for MPA

Table I shows the sensitivity and specificity of MPO-ANCA for the diagnosis of MPA using predetermined cut-off values of each ELISA system. Plasma samples from untreated MPA patients (n=52), disease controls (n=54) and healthy controls (n=55) were used in this study. The sensitivity and specificity were 90.4% and 98.2% (Nipro), 88.2% and 96.3% (MBL), and 86.5% and 99.1% (Wieslab) (Table I).

ROC analysis and AUC, MPO-ANCA for MPA

ROC was analysed with plasma samples from patients with untreated MPA patients (n=52), disease controls (n=54), and healthy control (n=55). The overall diagnostic performance, assessed as the area under curve (AUC) of the four MPO-ANCA ELISAs were 0.946±0.022 (Nipro), 0.970±0.017 (MBL), and 0.971±0.017 (Wieslab). There were no significant differences among these ELISAs using pairwise comparison of ROC curves (Table I).

Clinical diagnostic performance of PR3-ANCA for WG

Table II shows the sensitivity and specificity of PR3-ANCA for the diagnosis of WG using predetermined cut-off values of each ELISA system. Plasma samples from untreated WG patients (n=11), disease controls (n=54), and healthy controls (n=55) were used in this study. The sensitivity and specificity were 100.0% and 98.2% (Nipro), 100.0% and 95.4% (MBL), and 90.9% and 99.1% (Wieslab) (Table II).

ROC analysis and AUC, PR3-ANCA for WG

ROC was analysed with plasma samples from untreated WG patients (n=11), disease controls (n=54), and healthy control (n=55). The AUC of PR3-ANCA ELISAs were 0.986±0.025 (Nipro), 0.993±0.017 (MBL), and 0.916±0.059 (Wieslab). There were no significant differences among these ELISAs using pairwise comparison of ROC curves (Table II).

Correlation between MPO-ANCA ELISA systems

Correlations between MPO-ANCA ELISAs were analysed using 146 plasma samples from patients with PSV at various stages (MPA, n=132; CSS, n=1; WG, n=13). All data were $\log_{10}$ transformed to normalise distributions prior to this analyses. Nipro MPO-ANCA ELISA was positively correlated with MBL MPO-ANCA ($r=0.891$, $p<0.0001$, Fig. 1) and Wieslab MPO-ANCA ($r=0.879$, $p<0.0001$). MBL MPO-ANCA and Wieslab MPO-ANCA were positively correlated with each other ($r=0.899$, $p<0.0001$, Table III).

Percentage of ANCA positivity in patients with PSV

MPO-ANCA positivity in MPA was 86.5% (45/52) in Nipro ELISA, 80.8% (42/52) in MBL ELISA, and 82.7% (43/52) in Wieslab ELISA. PR3-ANCA positivity in MPA was 3.8% (2/52) both in Nipro and Wieslab ELISAs, and 7.7 % (4/52) in MBL ELISAs. Absence of ANCA in MPA was 7.7 % (4/52) both in Nipro and MBL ELISAs, and 9.6% (5/52) in Wieslab ELISA. PR3-ANCA positivity in WG was 100% (11/11) both in Nipro and MBL ELISAs, and 90.9% (10/11) in Wieslab ELISA. A CSS patient showed positive MPO-ANCA only in MBL ELISA (Table IV).